

Astroparticle Physics

Lectures:

- 05.02.2019 [1. Historical introduction, basic properties of cosmic rays](#)
- 07.02.2019 [2. Hadronic interactions and accelerator data](#)
- 19.02.2019 [3. Cascade equations](#)
- 21.02.2019 [4. Electromagnetic cascades](#)
- 26.02.2019 [5. Extensive air showers](#)
- 28.02.2019 [6. Detectors for extensive air showers](#)
- 09.04.2019 [7. High energy cosmic rays and the knee in the energy spectrum of cosmic rays](#)
- 16.04.2019 [8. Radio detection of extensive air showers](#)
- 25.04.2019** 9. Acceleration, astrophysical accelerators and beam dumps
- 07.05.2019 10. Extragalactic propagation of cosmic rays
- 16.05.2019** 11. Ultra high energy cosmic rays
- 21.05.2019 12. Astrophysical gamma rays and neutrinos
- 28.05.2019 13. Neutrino astronomy
- 04.06.2019 14. Gamma-ray astronomy

<http://particle.astro.ru.nl/goto.html?astropart1819>

lecture 14

Gamma-ray astronomy

*astrophysical production of gamma rays
has been discussed in lecture 12,
Gaisser chapter 11*

High-energy gamma rays

In addition to charged particles we obtain information on the high-energy universe from gamma rays.

$$E \sim 100 \text{ MeV} \rightarrow 50 \text{ TeV}$$

Production & interaction

1) **synchrotron radiation** of electrons in B fields

Depending on the energy of the electron and the strength of the B field, the energy of photons ranges from radio (meV) to ~ 10 MeV

$$E_\gamma \propto B^2 \gamma^2$$

radiation is polarized

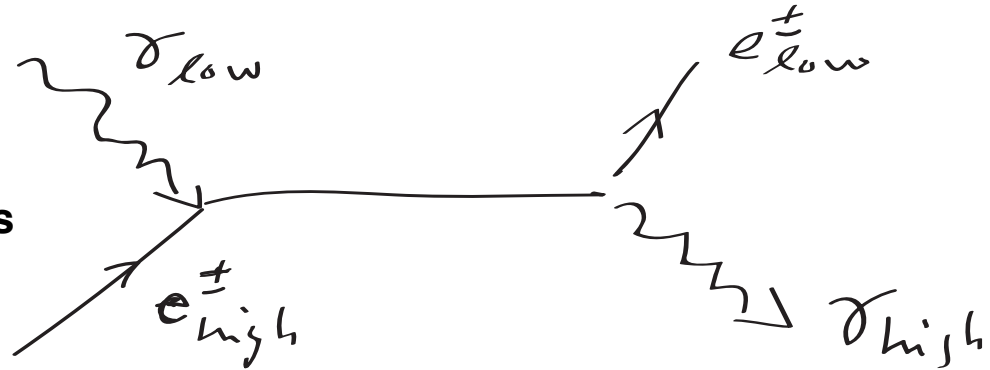


2) Inverse Compton scattering

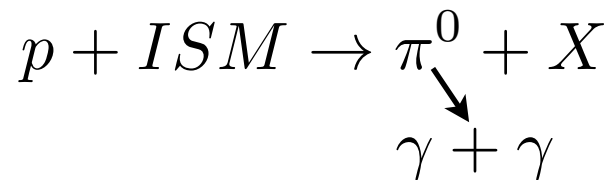
energy of electrons is transferred to photons
“heating of photons through electrons“

$$E_\gamma \propto U_{rad} \gamma_e^2$$

↑
temperature (kinetic energy) of photons



3) Hadronic interactions



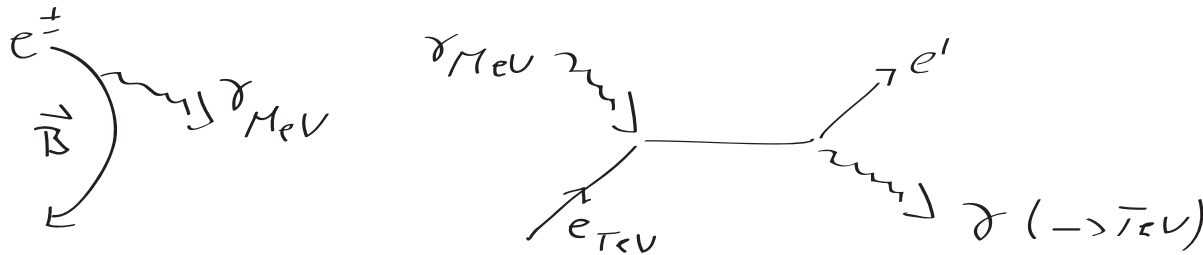
requires the presence of hadronic particles

4) Bremsstrahlung

e+target --> Bremsstrahlung

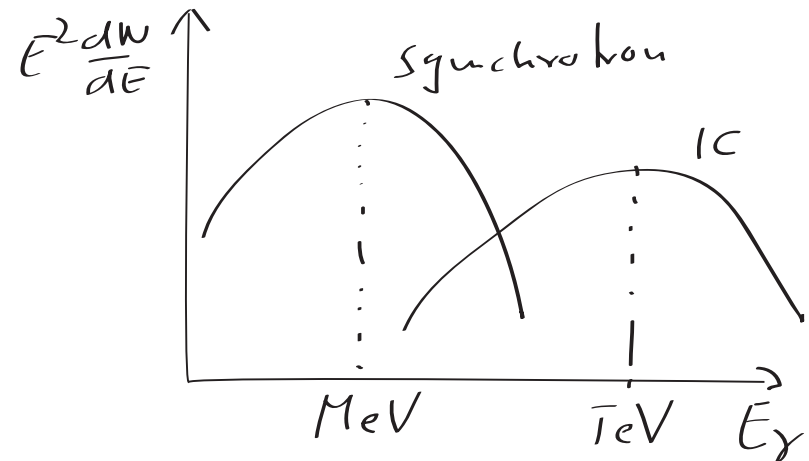
$$E_\gamma \approx \frac{E_e}{2} \text{ (power law)}$$

5) important combination of 1) and 2) synchrotron self compton (SSC)



the photons for inverse Compton scattering are produced in-situ

typical form of spectrum



Measurement of photons

1) detection in space

Fermi satellite

electromagnetic calorimeter

10 layers of Pb converter $\gamma \rightarrow e^+e^-$

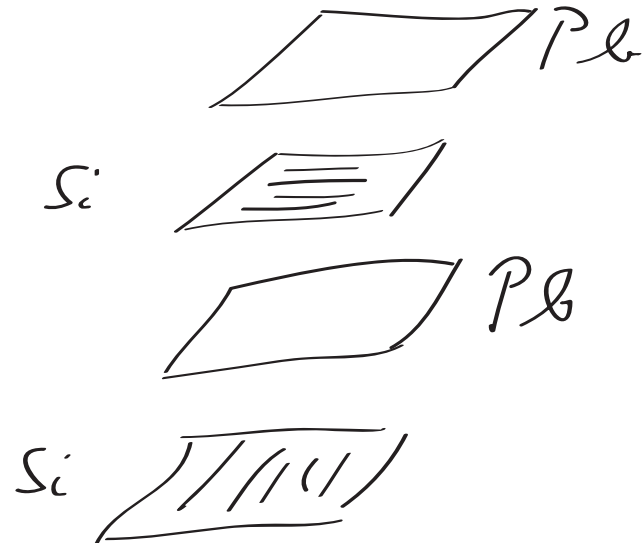
interspaced with 12 layers of Si strip detectors

electromagnetic cascade

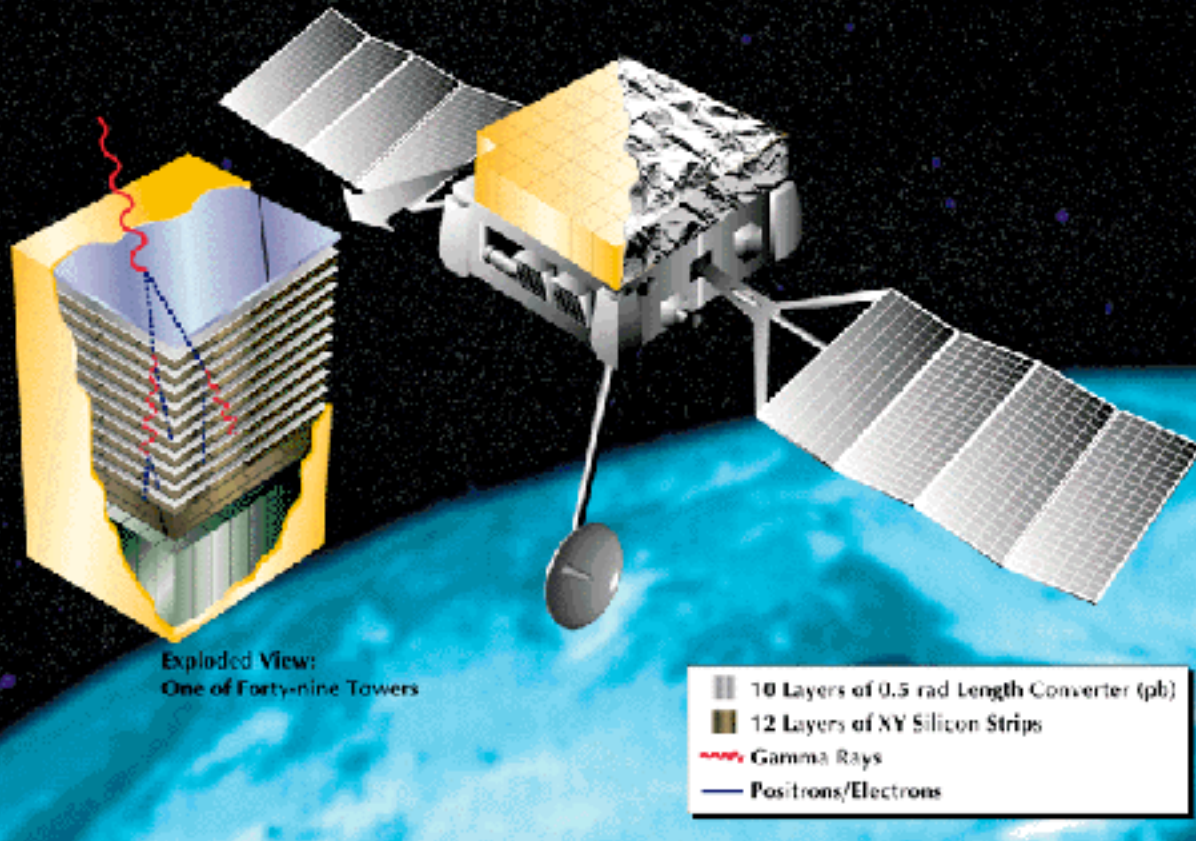
--> trajectory

--> $\sum E \rightarrow E_\gamma$

up to $E_\gamma \approx 10 - 20$ GeV



GAMMA-RAY LARGE AREA SPACE TELESCOPE



GLAST/Fermi



2) atmospheric Cherenkov telescopes

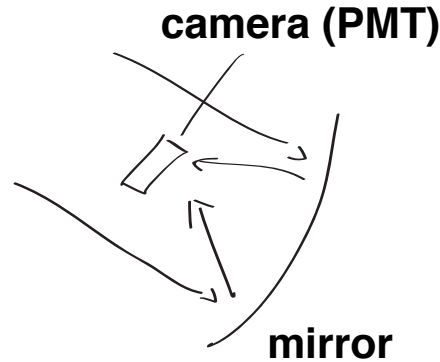
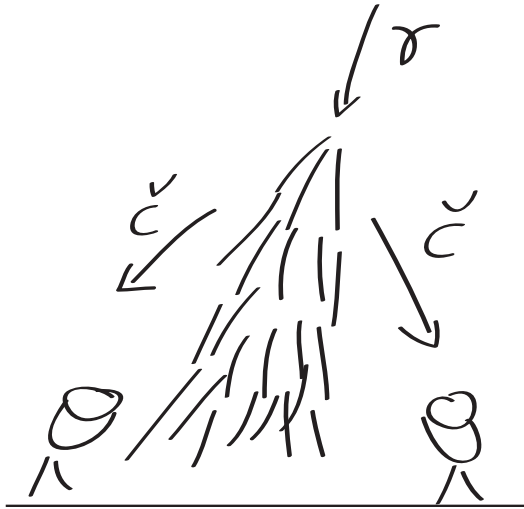


image of shower is recorded with a fast camera (PMT)

total number of photons $\rightarrow E_0$
field of view $\sim 4^\circ$

stereo observations

\rightarrow 3 dim trajectory of shower in atmosphere

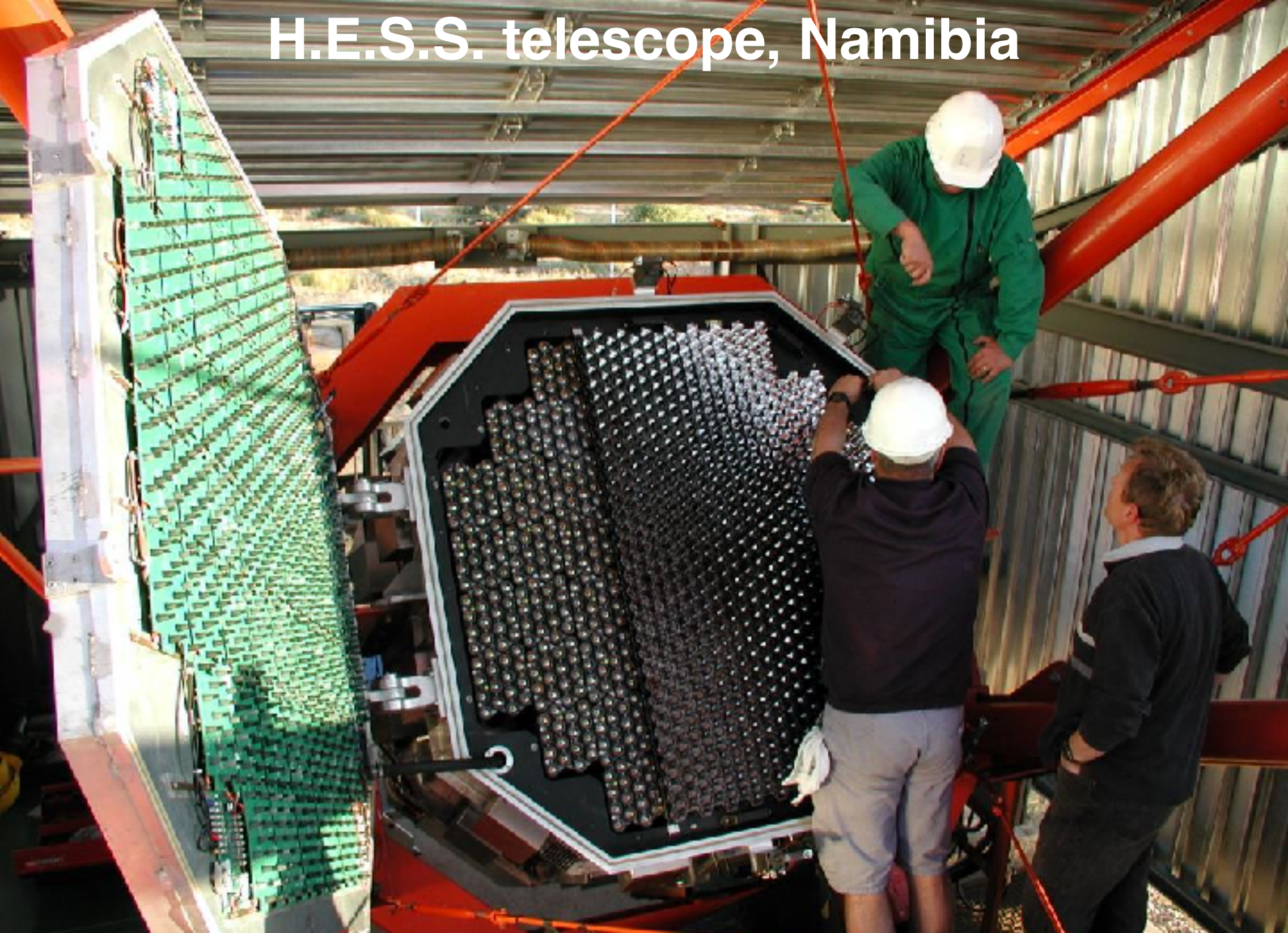
\rightarrow direction of the incoming photon

IACT = Imaging Atmospheric Cherenkov Telescope

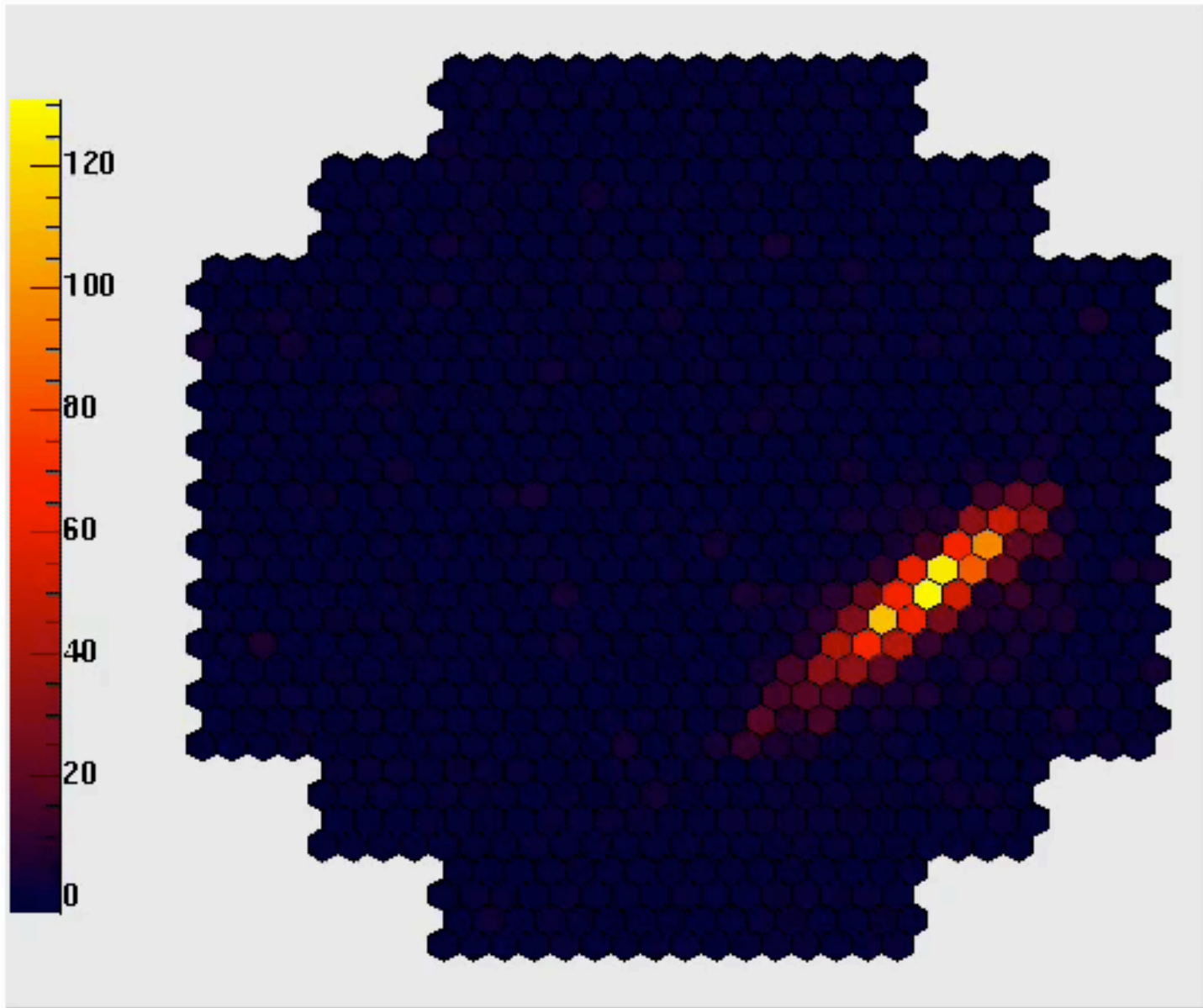
H.E.S.S. telescope, Namibia



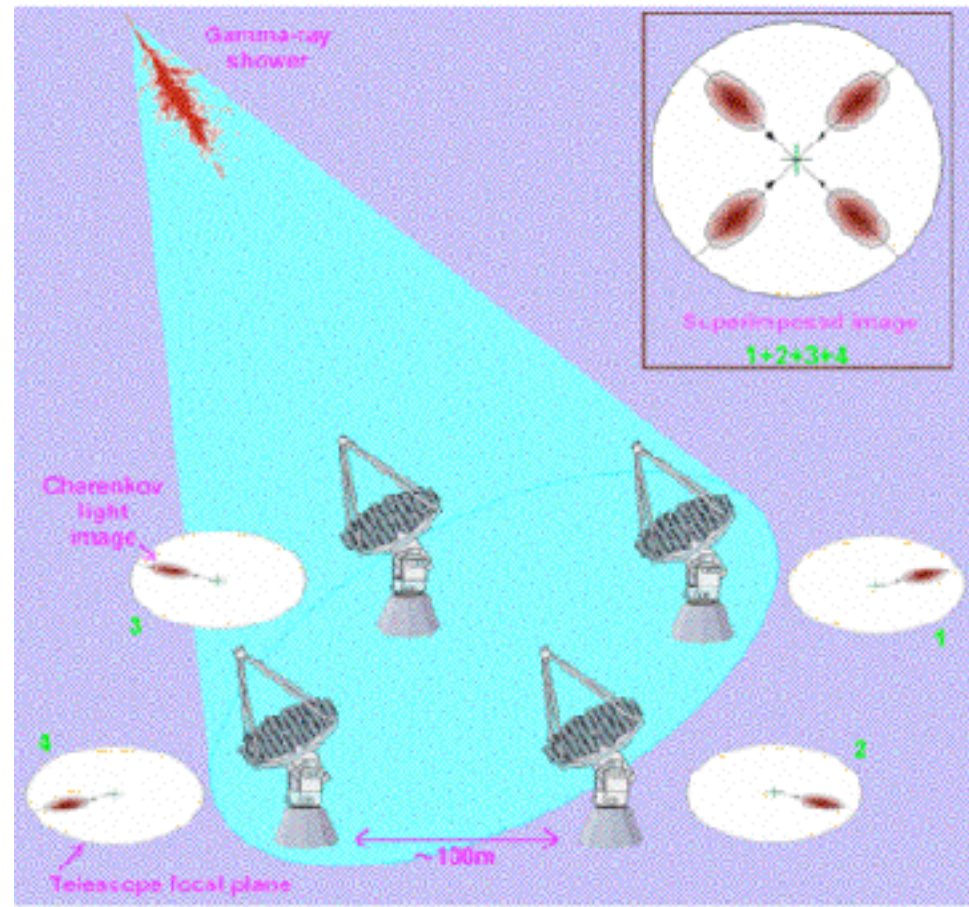
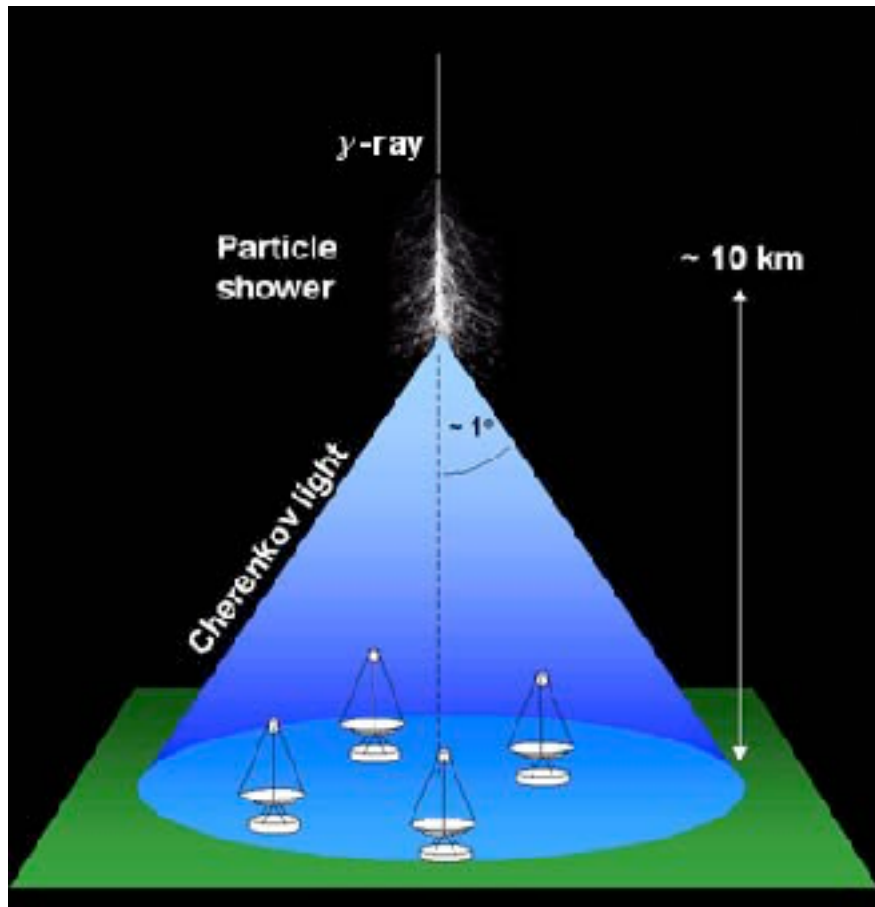
H.E.S.S. telescope, Namibia



H.E.S.S. telescope, Namibia



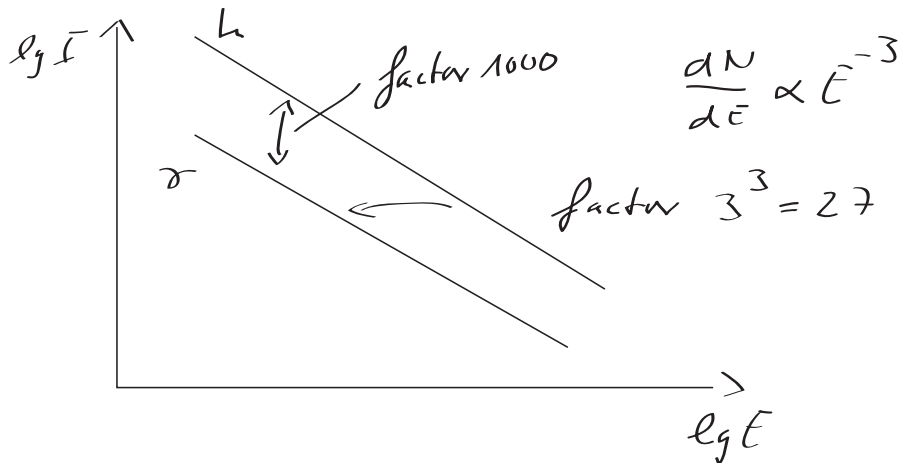
stereo observation



high background of hadronic particles

reduction through two effects:

- 1) hadronic particles produce only 1/3 Cherenkov light as photons of the same energy



hadronic particles at same number of Cherenkov photons are only $\frac{1000}{27} \approx 37$ times more abundant

- 2) pattern recognition in Cherenkov image

e/m cascades produce „smoother“ images

hadronic interaction length

vs

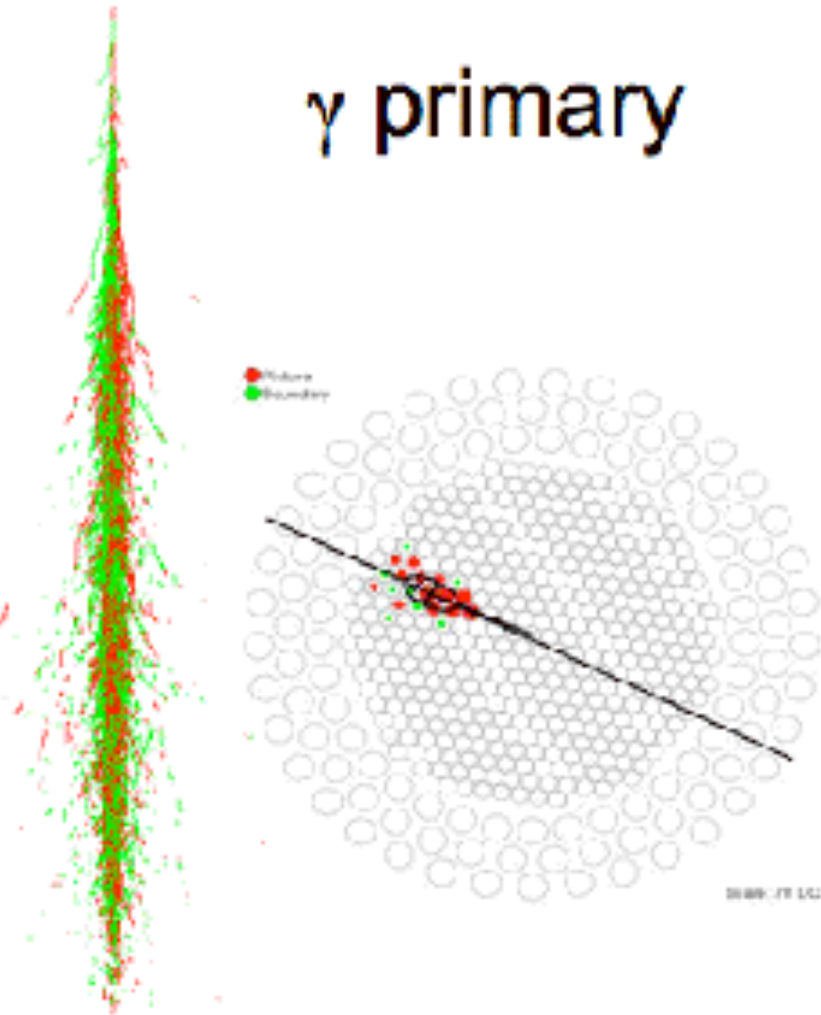
radiation length

$$\lambda_I = 90 \frac{\text{g}}{\text{cm}^2}$$

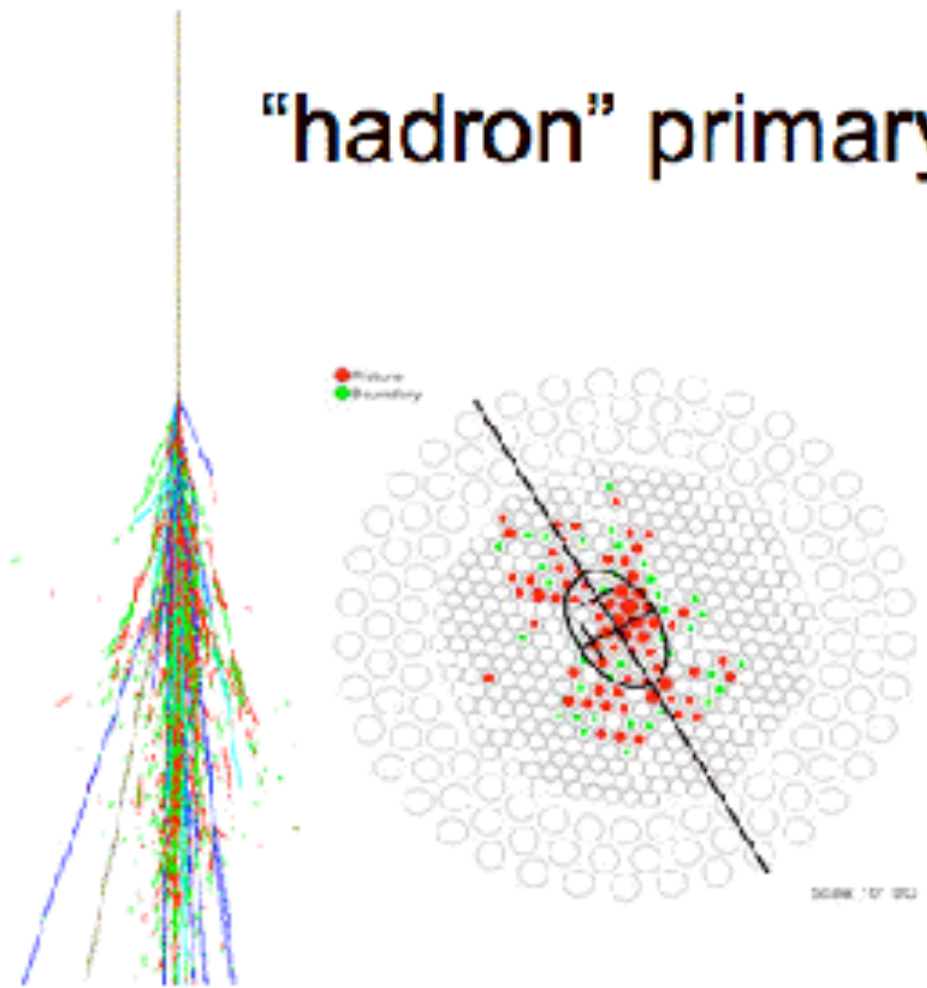
$$X_0 = 36 \frac{\text{g}}{\text{cm}^2}$$

gamma-hadron separation

γ primary

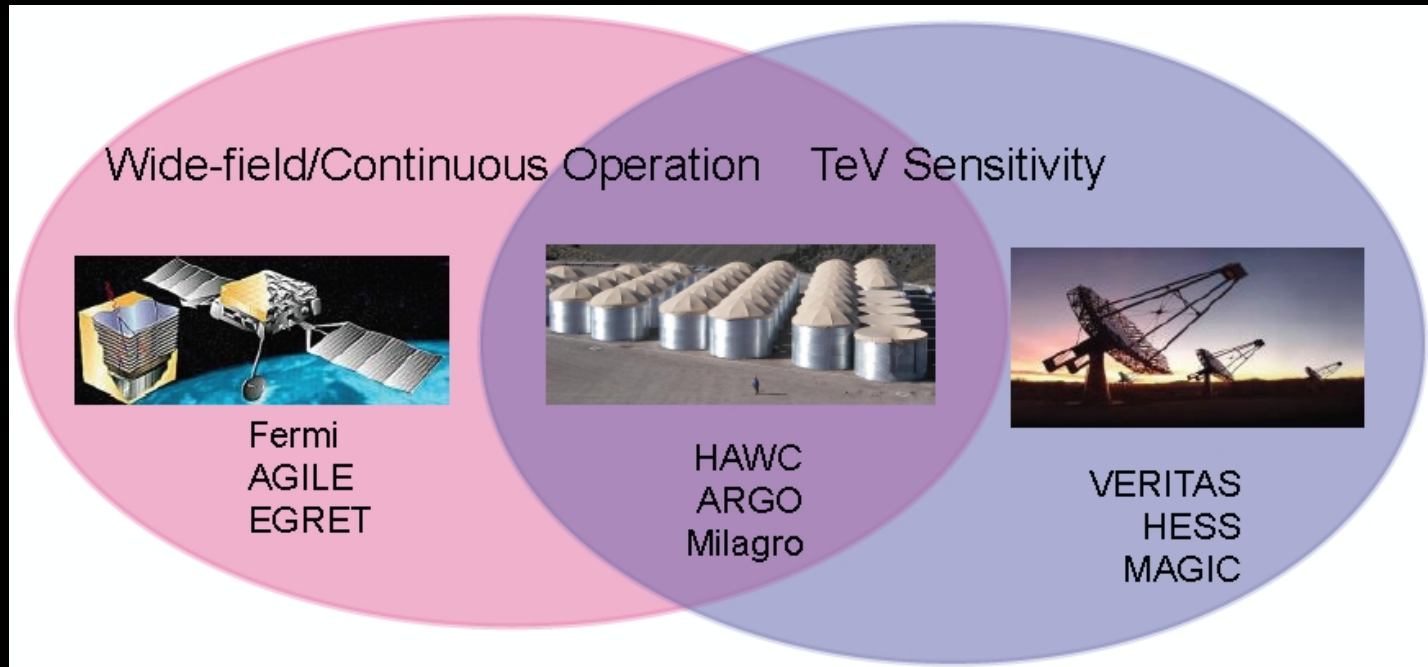


“hadron” primary

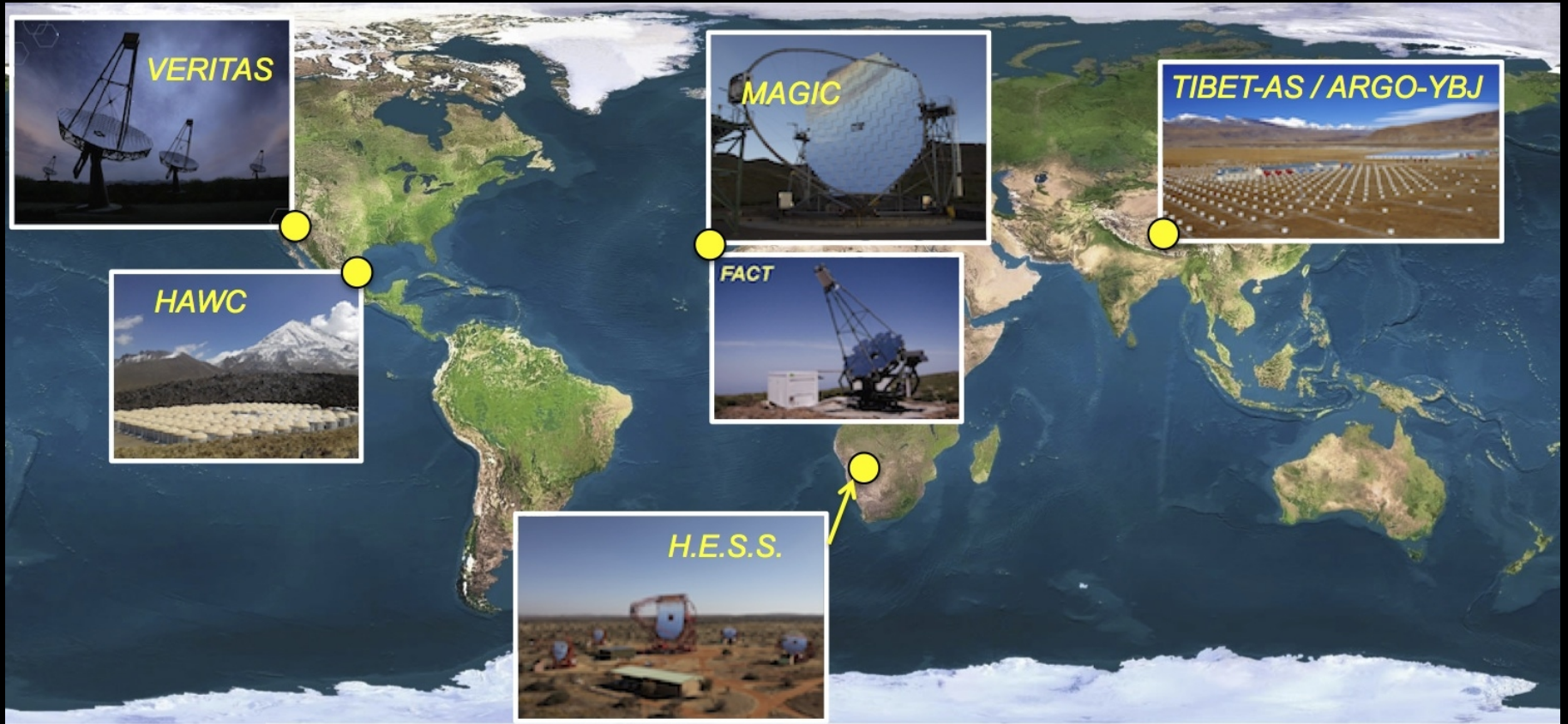


Complementarity of gamma-ray instruments

- Space-based detectors - continuous full-sky coverage in GeV
- Ground-based detectors have TeV sensitivity
 - Current Imaging Atmospheric Cherenkov Telescopes (IACTs) have excellent energy and angle resolution, but FoV of 0.003 sr and duty cycle of 10%
 - Particle detectors have an aperture > 2 sr and duty cycle of 90% but angular resolution of $\sim 0.6^\circ$ (@ 1 TeV)



INSTRUMENTS



Status of VERITAS

VERITAS has been operating smoothly since 2007 with 4 12m IACTs

Two major upgrades since inauguration:

In 2009, relocation of one of the telescopes

In 2011-2012, replaced the L2 trigger system and new high efficiency PMTs

Since fall 2012, observations carried out under bright moonlight: **detection of flaring activity from the BL Lac object 1ES 1727+502**

Energy range: 85 GeV to > 30 TeV

Sensitive to 1% Crab in ~ 25 hours

Angular resolution $\sim 0.1^\circ$ (68% containment)

VERITAS Highlight, 90, 676, 762



Status of MAGIC II

MAGIC is a system of two 17m diameter IACTs located at 2200m at La Palma
2 major upgrades in 2011-2012 (Camera, Data Acquisition)

During Winter 2013-2014, a new system (sum-trigger) was implemented for stereoscopic observations after several years of development

$E_{\text{threshold}}$ (trigger): ~ 50 GeV

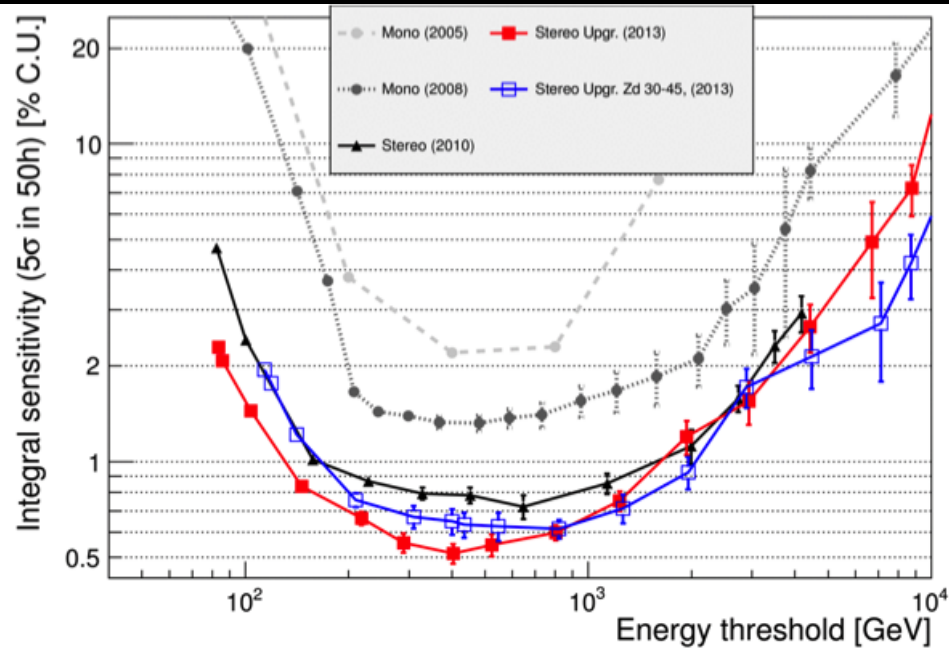
$E_{\text{threshold}}$ Sum-Trigger: ~ 35 GeV

Energy resolution: (15-20) %

Angular resolution: (0.05-0.1) $^{\circ}$

Sensitivity: $\sim 0.6\%$ Crab/50h

MAGIC Highlight, 60, 68, 101, 579



Status of H.E.S.S. II

HESS is an array of four 12m IACTs + one 28m telescope (CT5, FoV $\sim 3.5^\circ$)

CT5 is operational since 2012

Energy range from 30 GeV to 100 TeV

Focus system of CT5 under study \Rightarrow Focusing close to the altitude of shower maximum maximizes the γ -ray acceptance close to the energy threshold

Major upgrade of HESS I camera from 2015-2016: reducing the dead time of the cameras, improving the overall performance of the array and reducing the system failure rate related to aging

62, 98, 107, 108, 1011, 1046



Status of HAWC

HAWC Highlight, 96, 112, 418, 529, 692, 716, 739, 829

Array of water Cherenkov detectors (WCDs) spread on a 22 000 m² area

Located on the slope of the Sierra Negra Volcano in Mexico

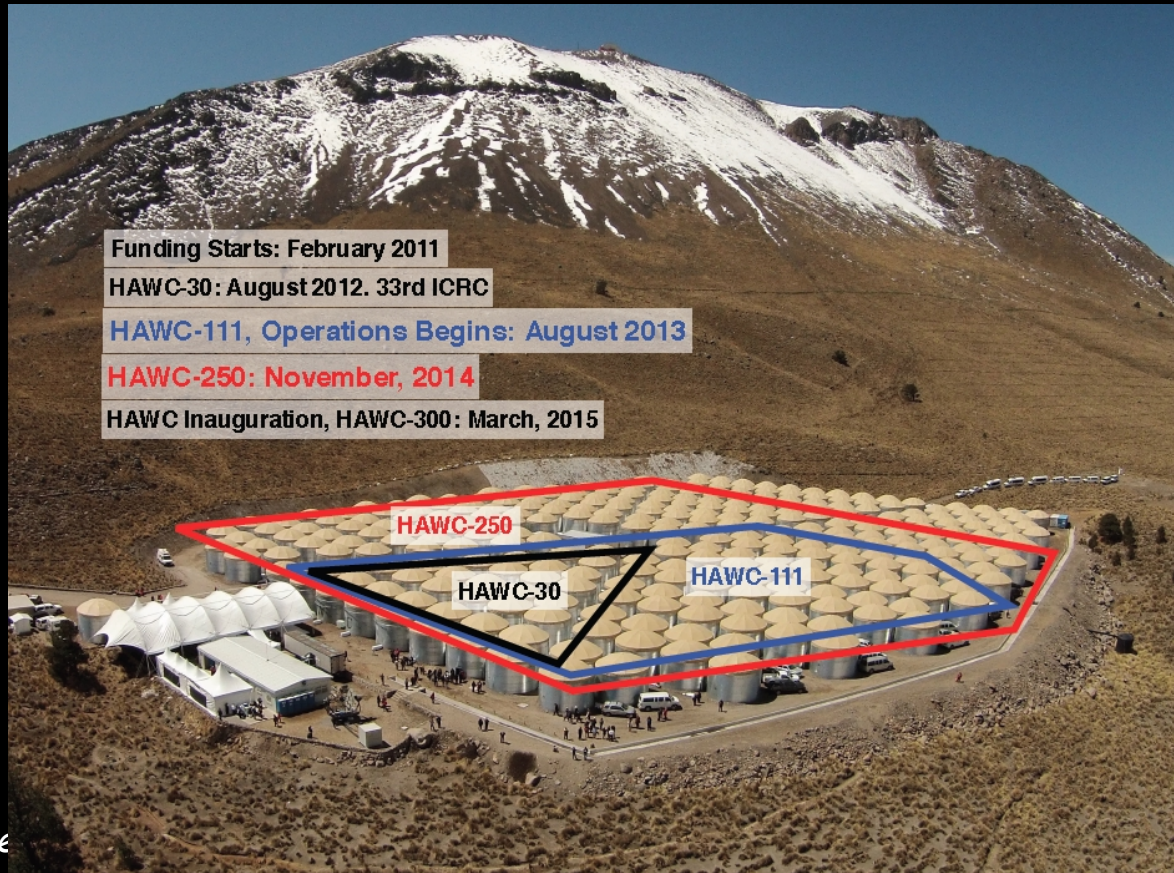
HAWC construction ended in March 2015 but data collection started already 2 years before, producing the first scientific results

HAWC Inauguration, HAWC-300: March, 2015

100 GeV - 100 TeV Sensitivity

Public data release
of all-sky data in 2017

HAWC Sparse Outrigger
Array: Enhanced Sensitivity
above 10 TeV



Status of ARGO-YBJ

Tibet, China, 4300 m above sea level
Full coverage with RPC detectors

849, 162

Large field of view

Zenith angle $< 50^\circ$

Survey of the Galactic plane at $25^\circ < l < 100^\circ$ and $130^\circ < l < 200^\circ$

Energy threshold

300 GeV \Rightarrow Overlaps the Fermi-LAT energy range

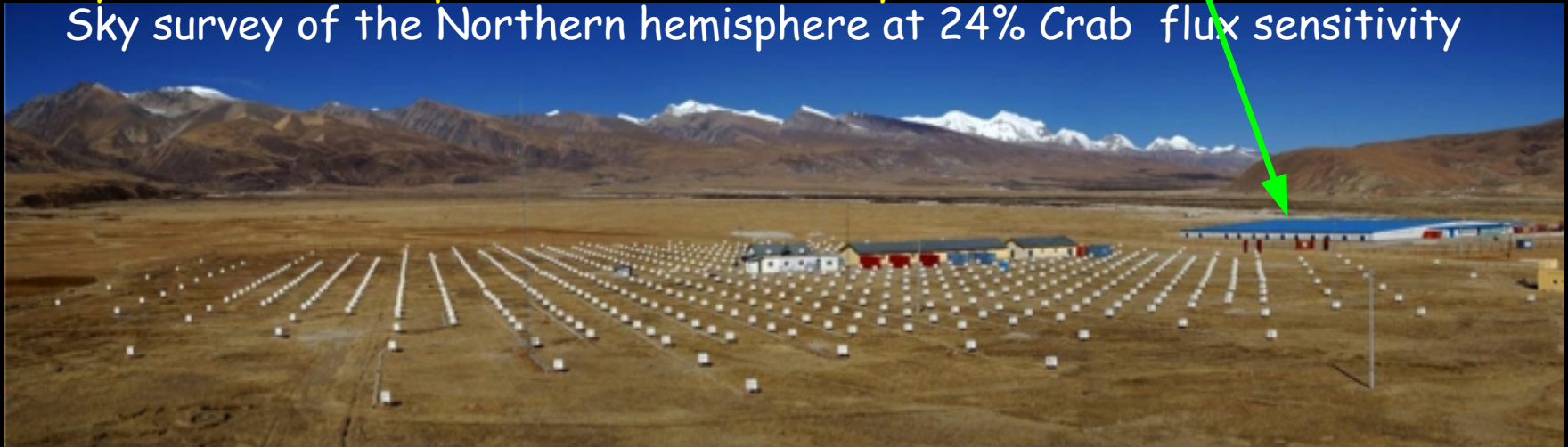
Angular resolution

0.99° for $N_{pad} > 100$

Five years of stable operation until February 2013

Sky survey of the Northern hemisphere at 24% Crab flux sensitivity

ARGO-YBJ



Status of Tibet ASy + MD

426, 452,
953, 1181

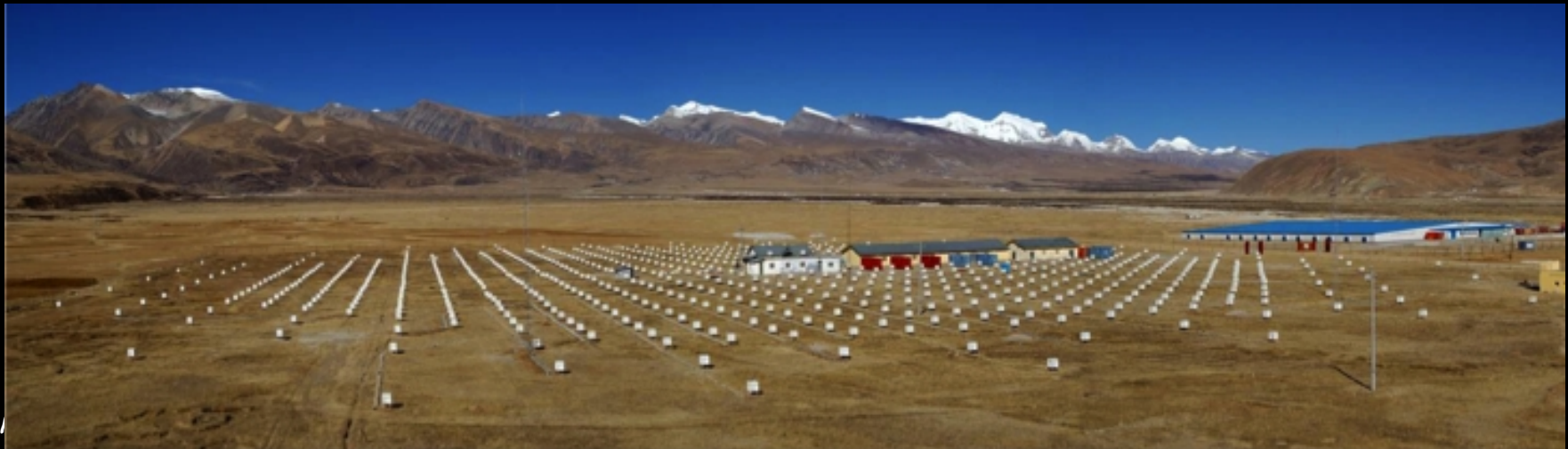
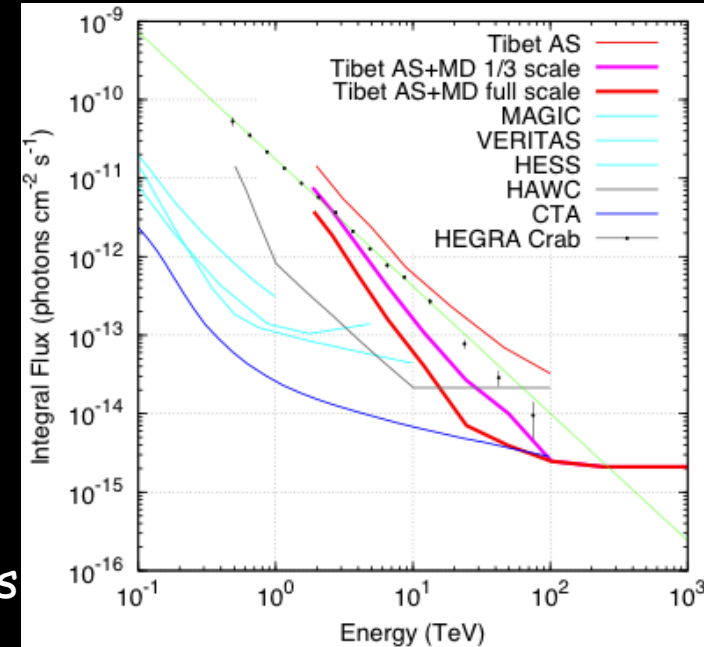
37000m² air shower particle detector array

789 scintillator detectors, at 4300m a.s.l.

Tibet III in operation since 1999

Energy interval: ~TeV to 100 PeV
Angular resolution: ~0.2° @ 100 TeV

Muon detector array under construction:
data taking has started with 5/12 since 2014
reduce background CRs by selecting γ -like events



The Cherenkov Telescope Array (CTA)

46, 47, 58, 61, 62, 63, 65, 78, 83, 202, 204, 209, 210, 236, 249, 252, 264, 265, 274, 276, 294, 305, 318, 329, 370, 372, 395, 424, 465, 469, 506, 556, 603, 605, 610, 629, 665, 673, 674, 684, 699, 723, 736, 773, 824, 862, 882, 900, 954, 965, 1052, 1057, 1058, 1101, 1179, 1319, 1324, 1397

> 1200 members

194 Institutes from 31 countries

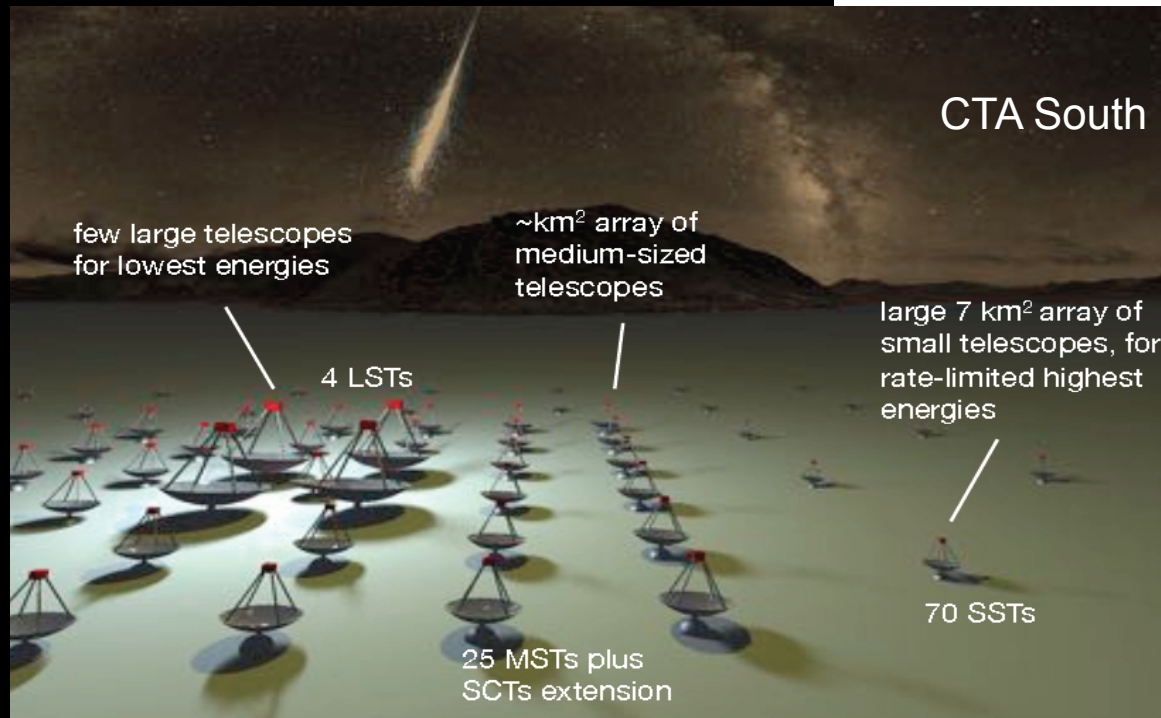
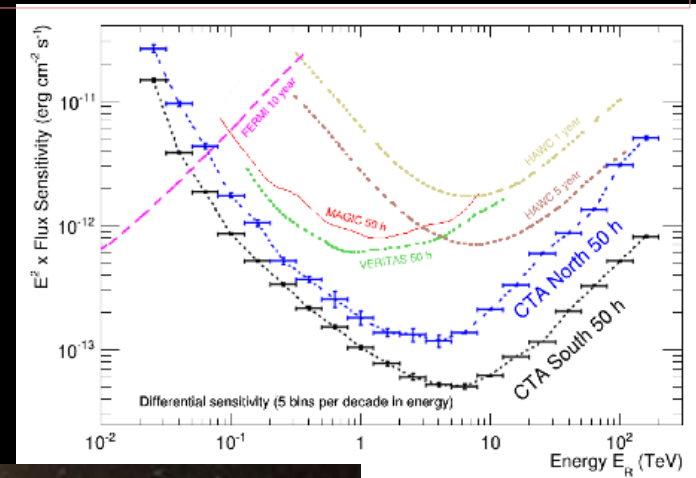
2 sites selected:

North (La Palma, Spain)

South (Paranal, Chile)

Initial construction could start in 2016

Early science: towards the end of the decade



diffuse gamma radiation

1) **radio** wavelengths

synchrotron radiation from electrons in B fields

intensity $\propto B\rho_e$

halo of galaxies are more extended than the visible region

--> confirmation that **cosmic rays (electrons)**
propagate in the galactic halo

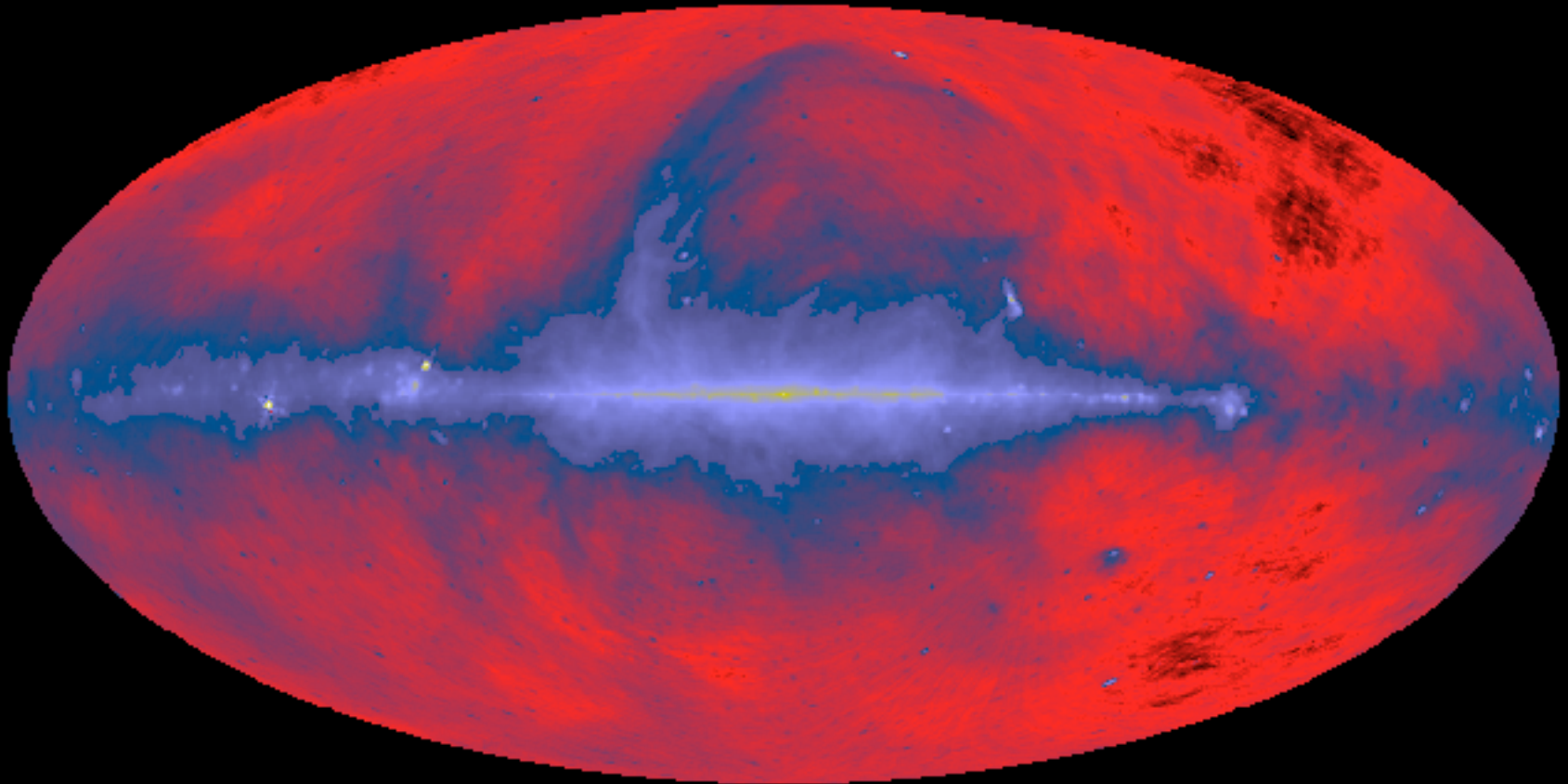
2) also diffuse **gamma radiation** observed $E > 100$ MeV

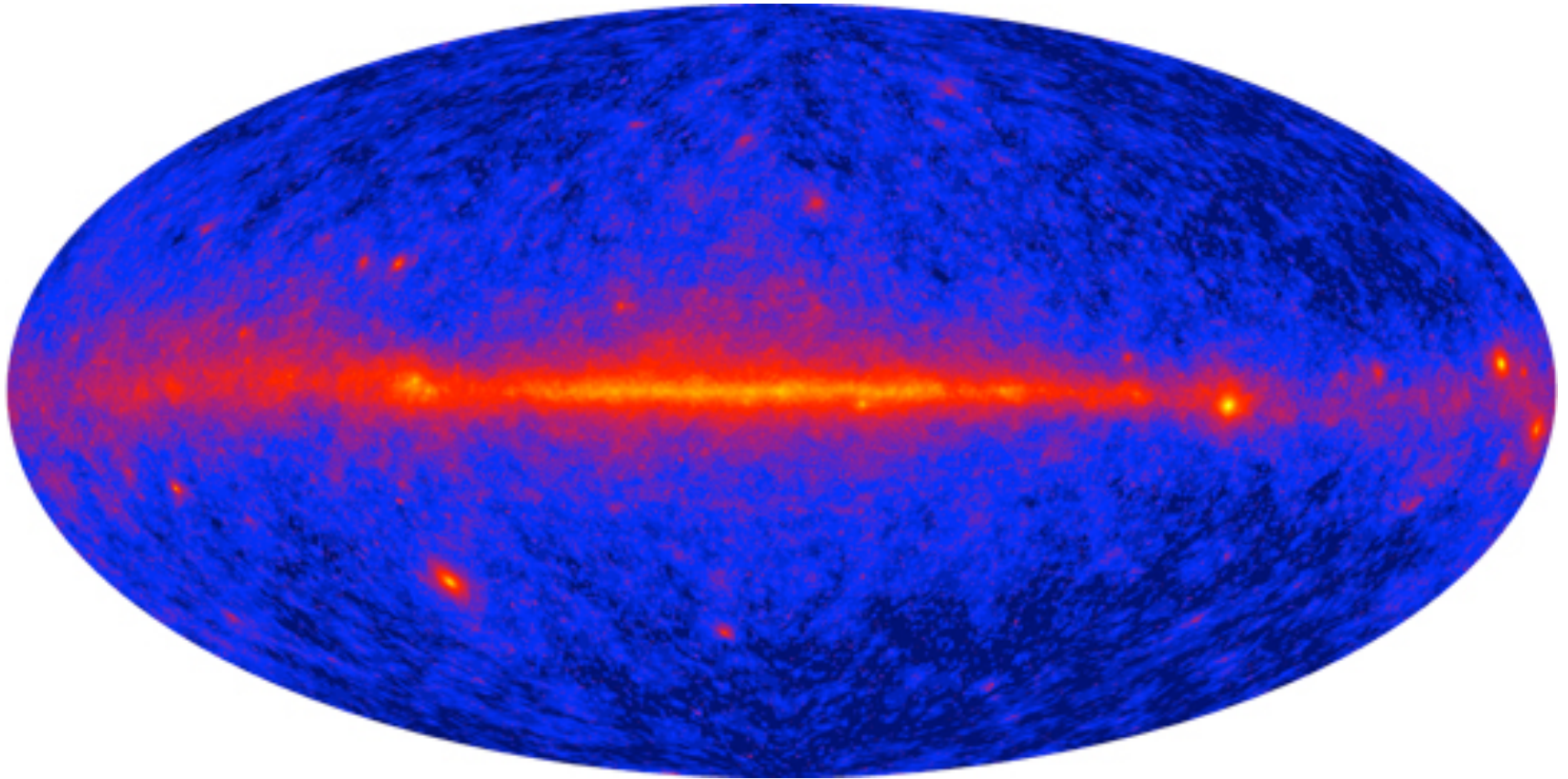
origin: $CR + ISM \rightarrow \pi^0 \rightarrow \gamma + \gamma$

--> **direct hint that cosmic rays (hadrons) are not a local phenomenon**

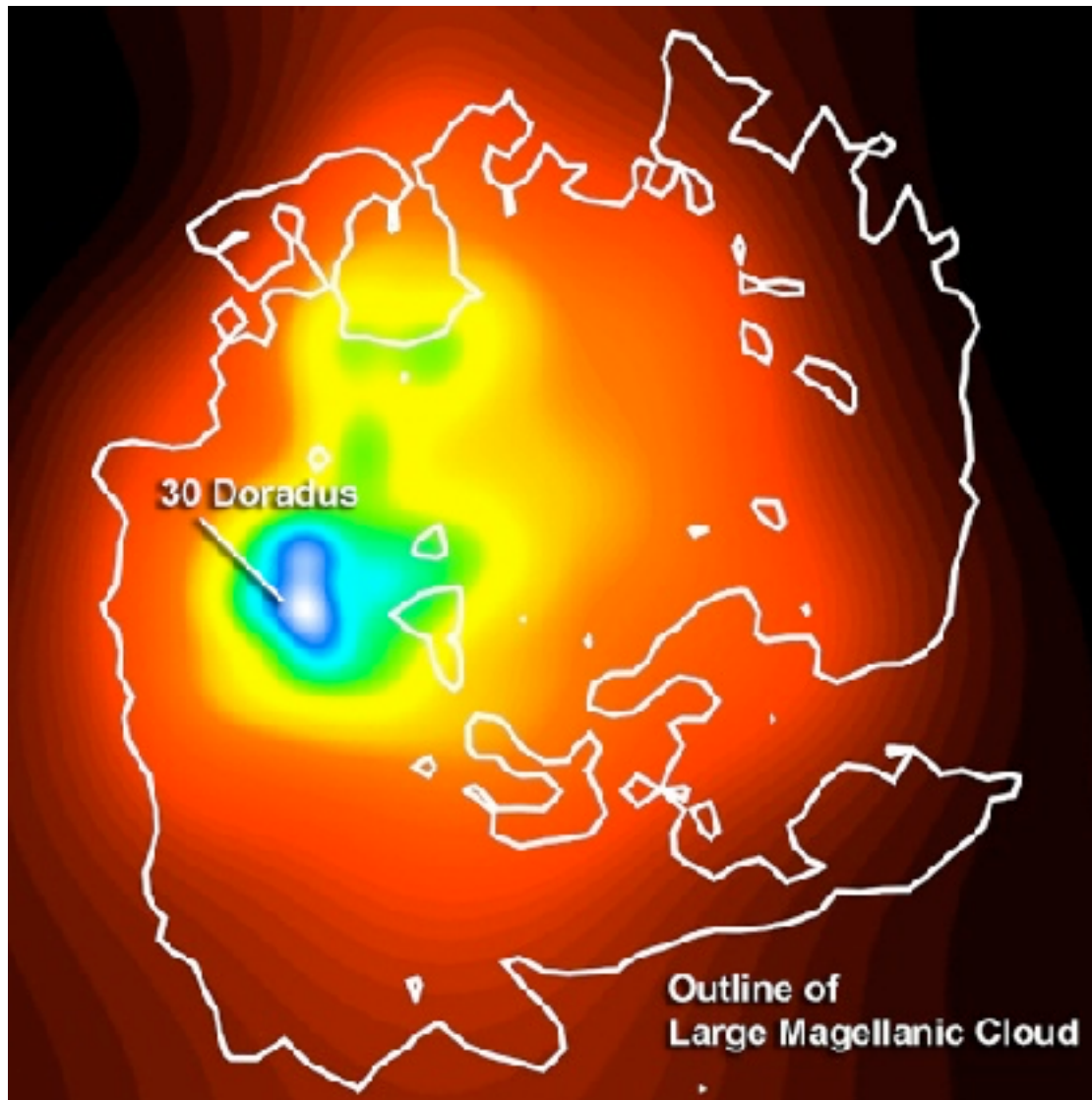
they propagate in the halo of the Milky Way and they exist in other galaxies

diffuse **radio** background of the Milky Way





The Fermi All Sky Map, showing the diffuse galactic
gamma-ray background from the Milky Way.
Courtesy of NASA/DOE/International LAT Team



Fermi's Large Area Telescope shows that an intense star-forming region in the **Large Magellanic Cloud** named 30 Doradus is also a source of **diffuse gamma rays**. Brighter colors indicate larger numbers of detected gamma rays.

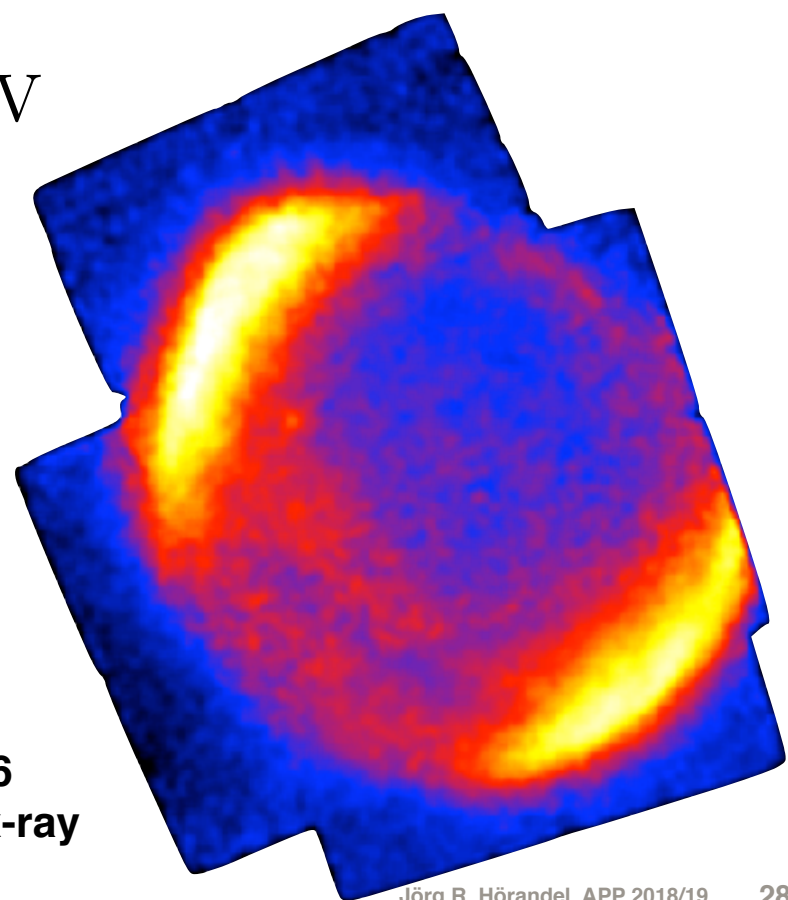
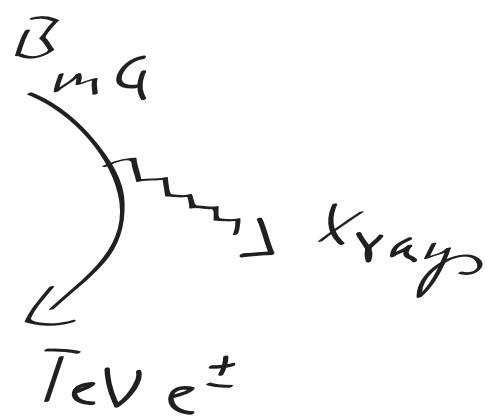
point sources

1) galactic sources supernovae

1995 first hint that electrons are accelerated in B fields of SNR

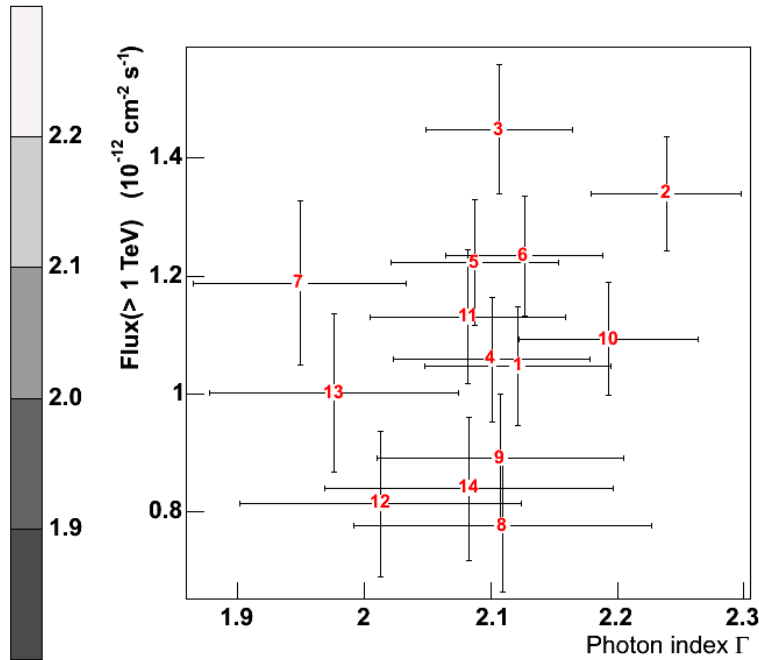
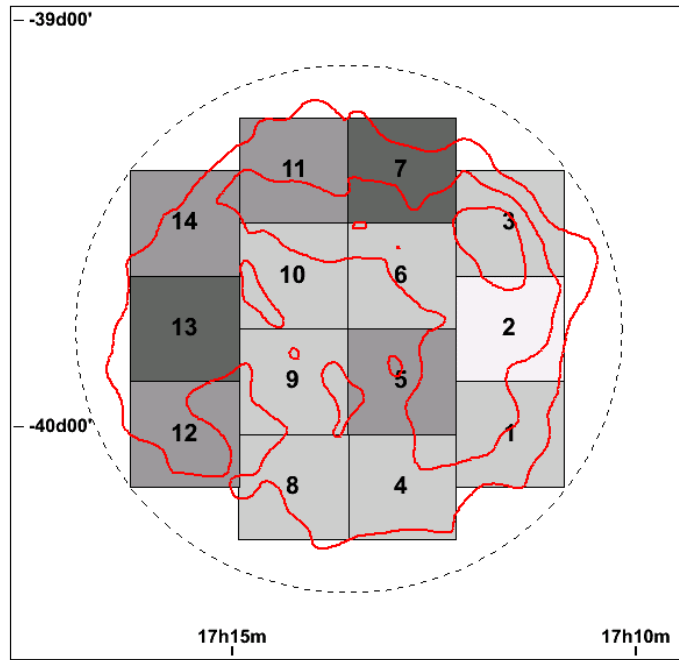
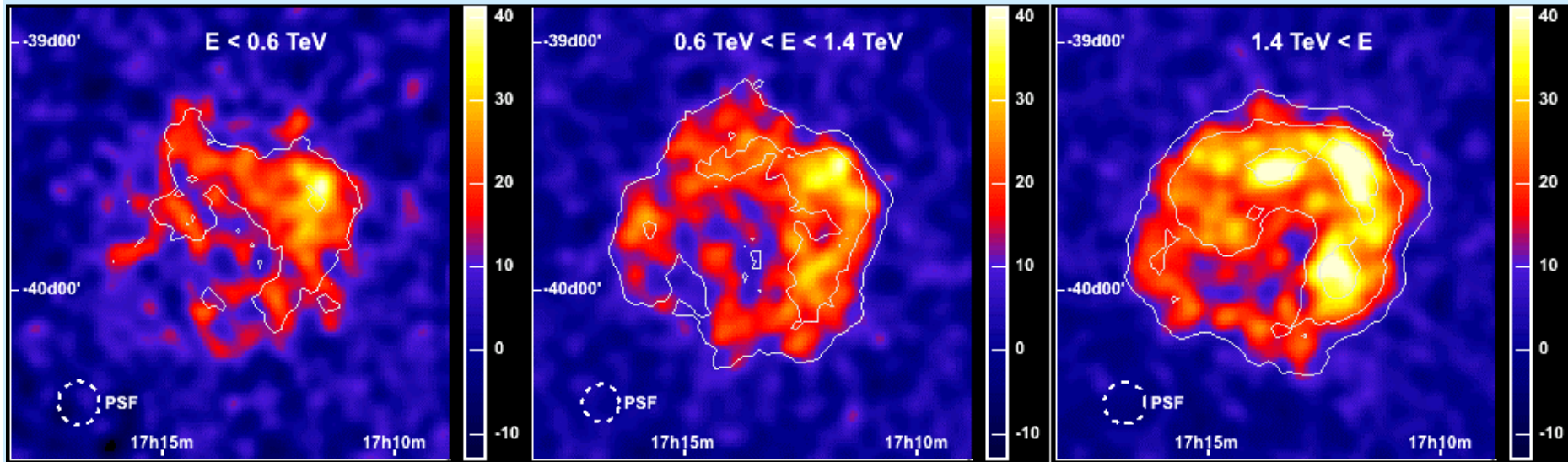
synchrotron radiation
from x-ray spectrum

$$\rightarrow E_e \approx \text{TeV}$$



SN 1006
ASCA x-ray

H.E.S.S. supernova remnant RXJ 1713



**spectral index
as expected
from 1st order
Fermi
acceleration ~
-2.1**

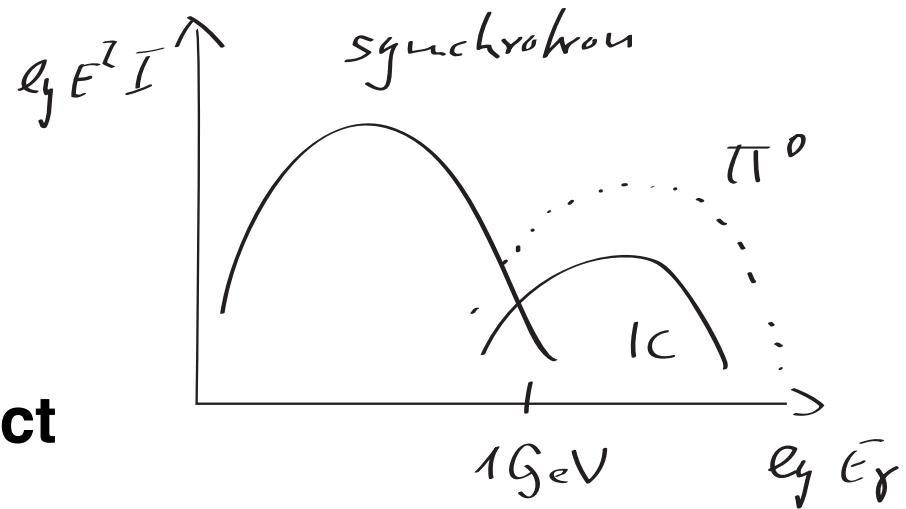
2004: H.E.S.S. telescopes observation of SNR RXJ1713

observed spectrum:

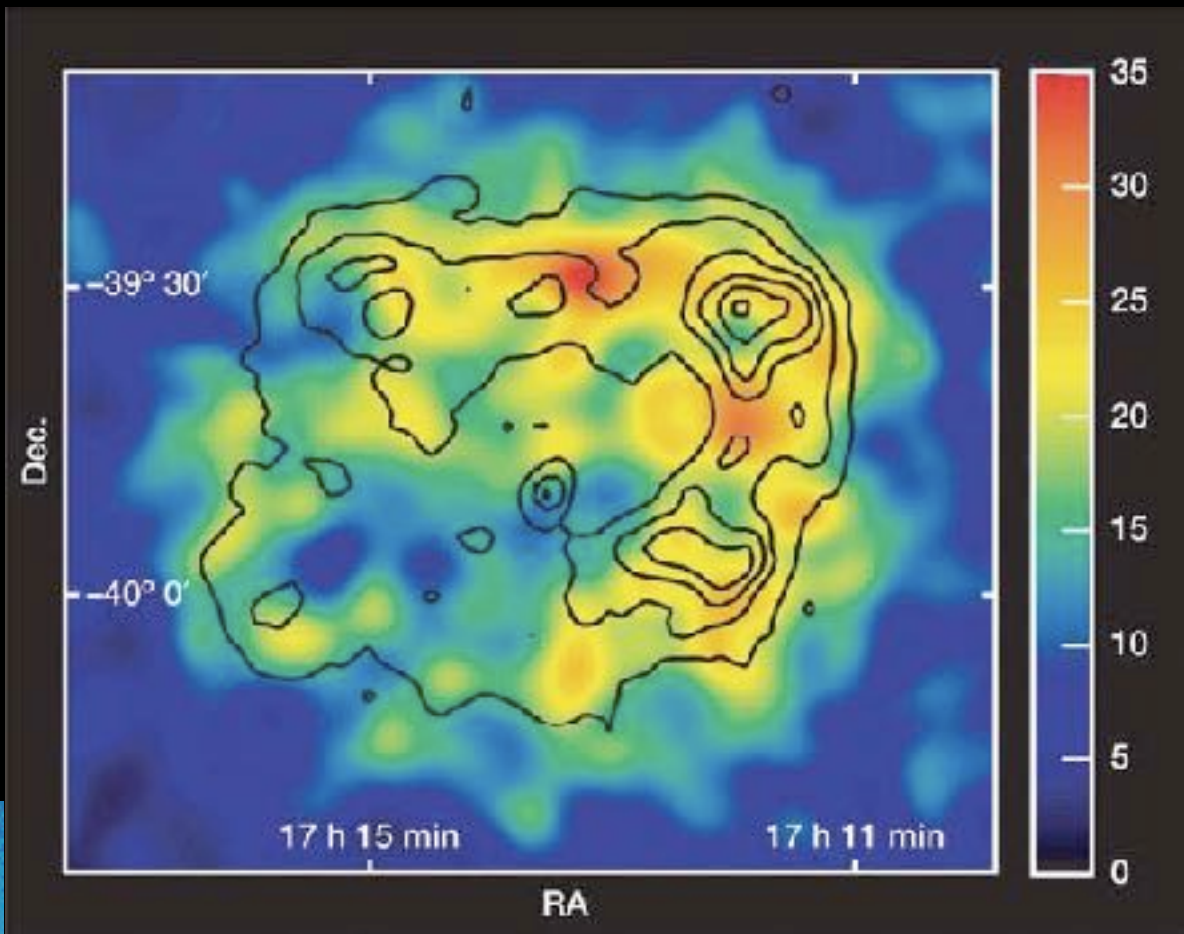
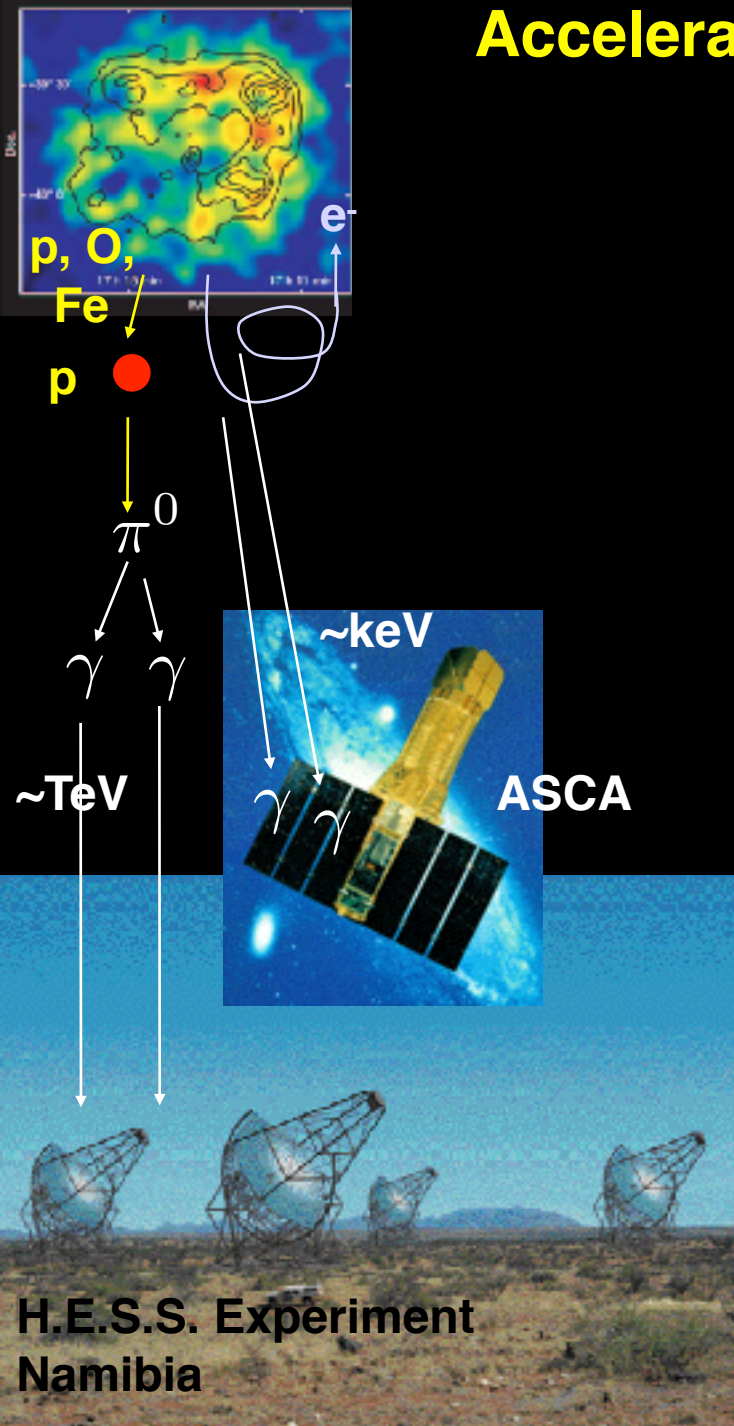
- acceleration of electrons:
SSC, i.e. inverse Compton effect
of γ s on TeV electrons

- acceleration of hadrons (nuclei):
 γ s originate from π^0 decay

which process dominates?

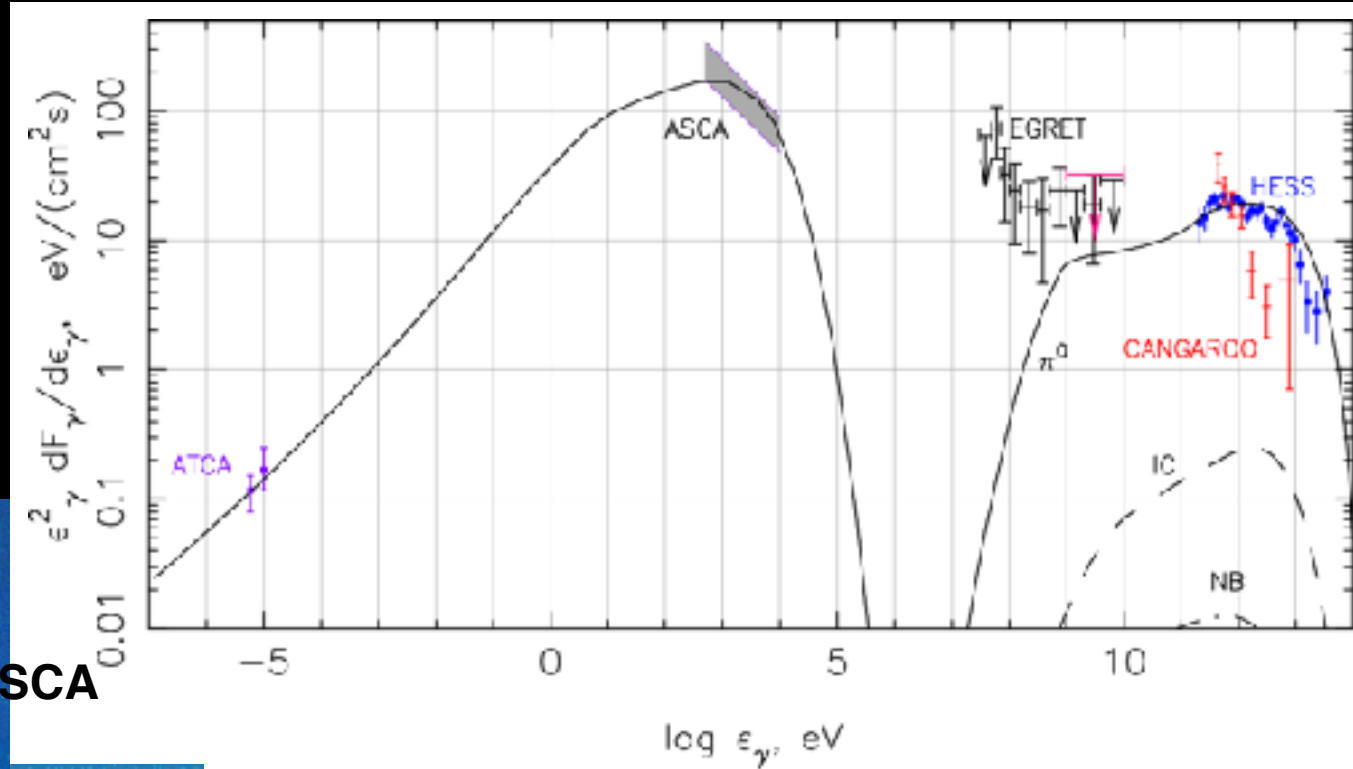
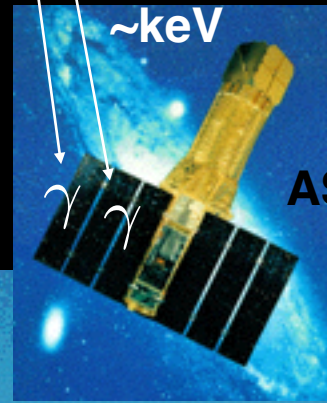
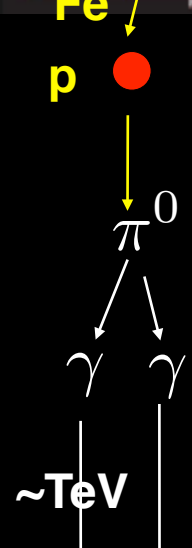
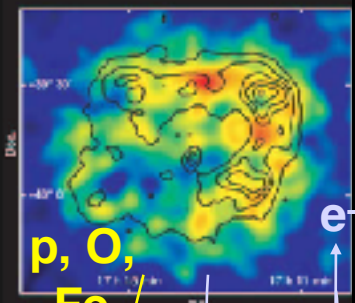


Acceleration of particles in supernova remnant



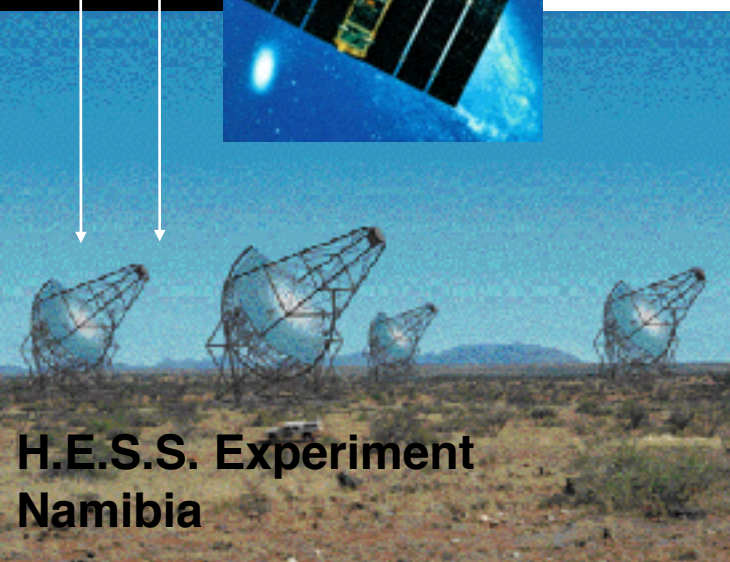
SNR RX J1713.7-3946
 H.E.S.S.: TeV-Gamma rays
 ASCA: X-rays (keV)

Acceleration of particles in supernova remnant



H. Völk & E.G. Berezhko, A&A 451 (2006) 981

SNR RX J1713.7-3946
 H.E.S.S.: TeV-Gamma rays
 ASCA: X-rays (keV)



Acceleration of hadrons (H. Völk et al)

Accelerated cosmic rays modify the B field at the SNR (self amplification)

--> B field in SNR is (much) larger than in ISM

$\sim 100 \mu\text{G}$ instead of $\sim 3 \mu\text{G}$

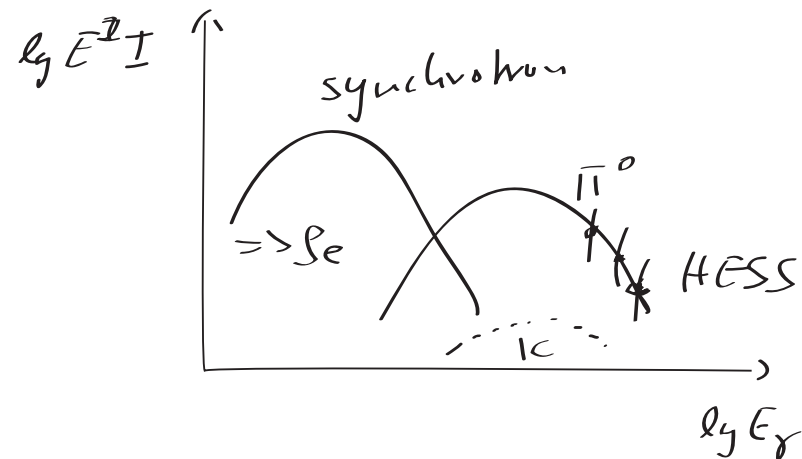
--> effective production of synchrotron radiation

--> observed flux of x rays and radio can be explained by a moderate electron number density

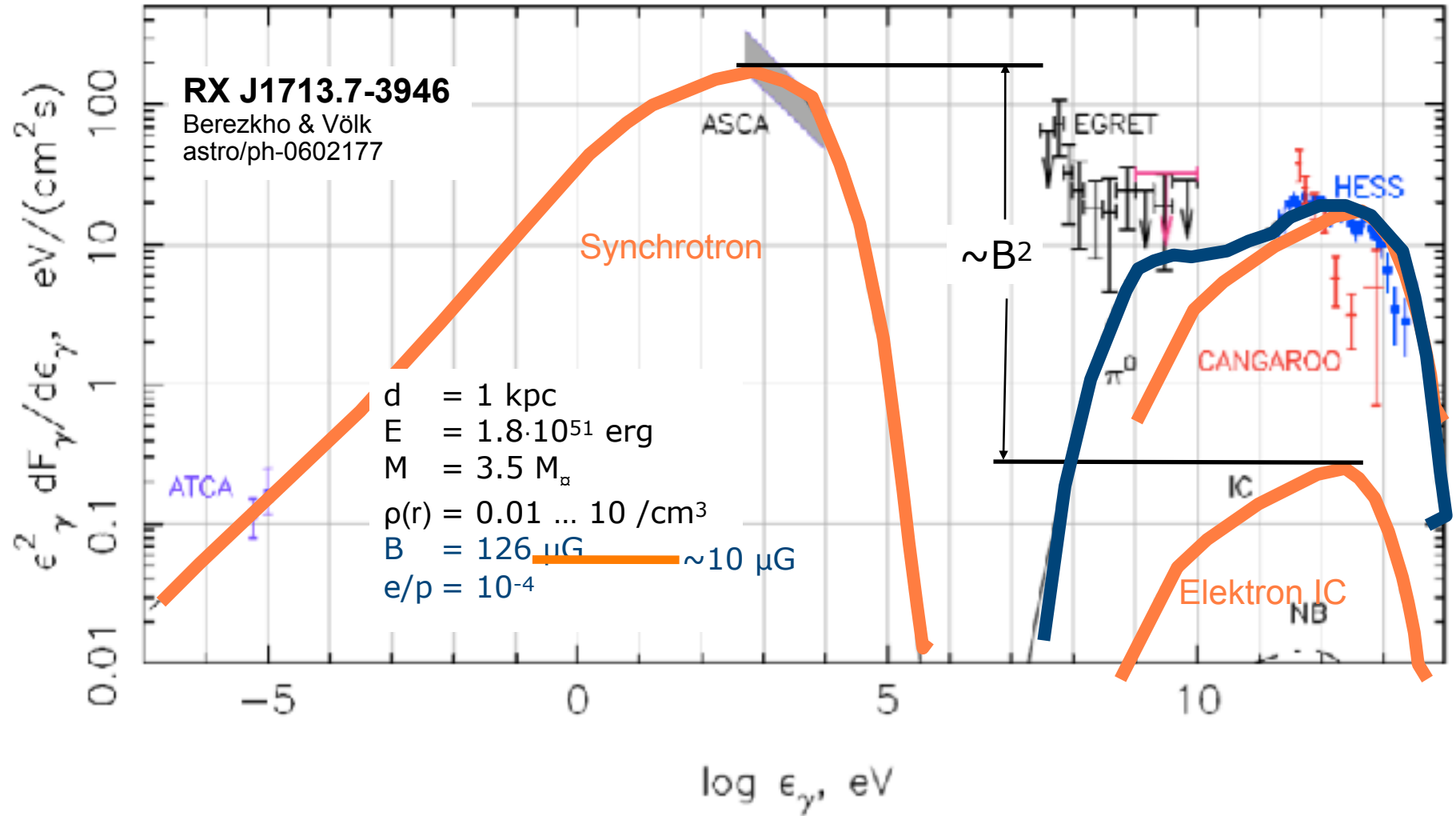
--> fraction of inverse Compton contribution is relatively small

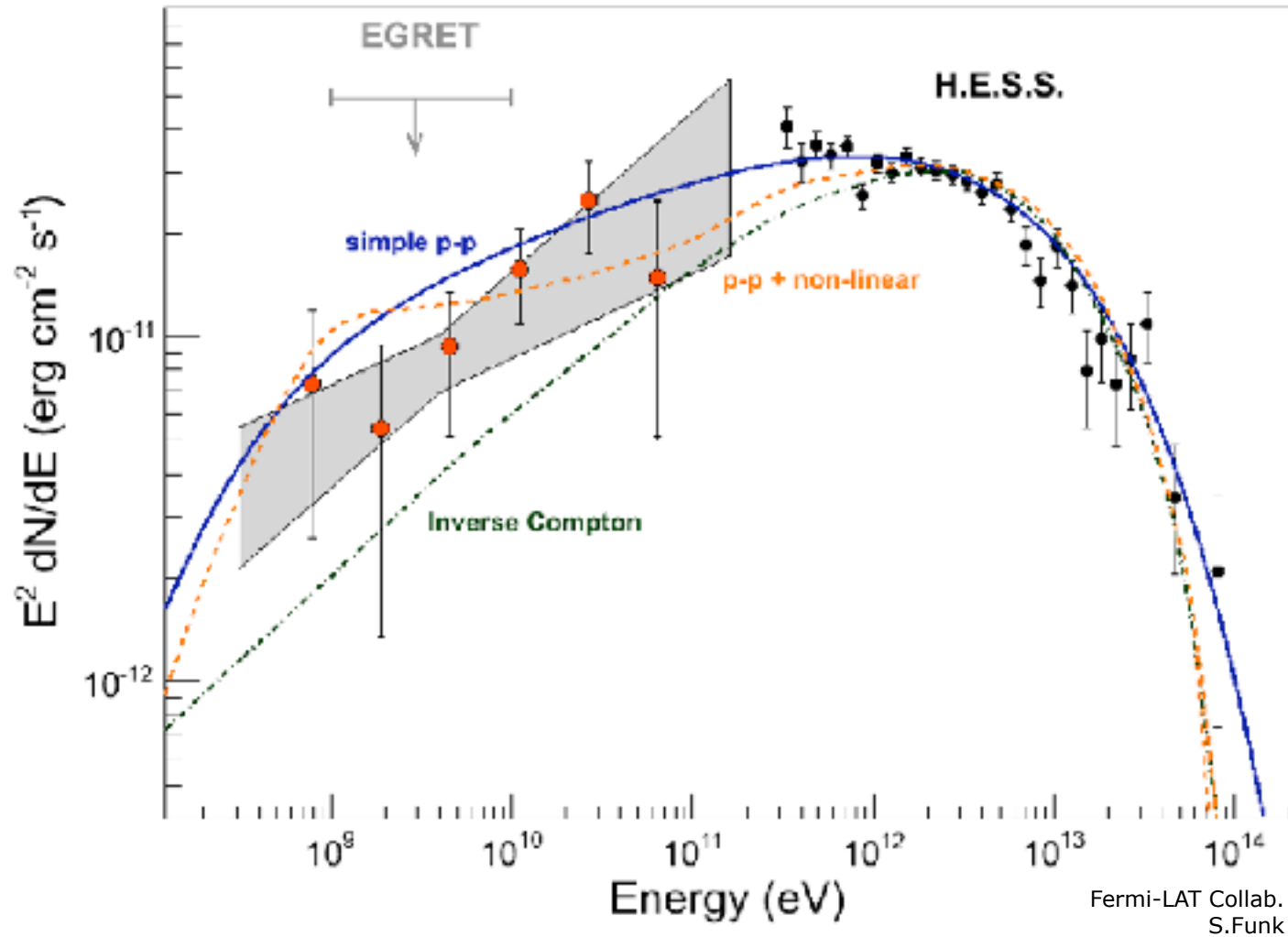
--> most likely the observed TeV gamma rays are from π^0 decay

--> hint for the acceleration of hadrons in SNR



BUT: is self amplification realized in nature?





Fermi-LAT Collab.
S.Funk

The supernova remnant W44: Confirmations and challenges for cosmic-ray acceleration

M. Cardillo^{1,2}, M. Tavani^{1,2,3}, A. Giuliani^{3,4}, S. Yoshiike⁵, H. Sano⁵, T. Fukuda⁵, Y. Fukui⁵,
 G. Castelletti⁶, and G. Dubner⁶

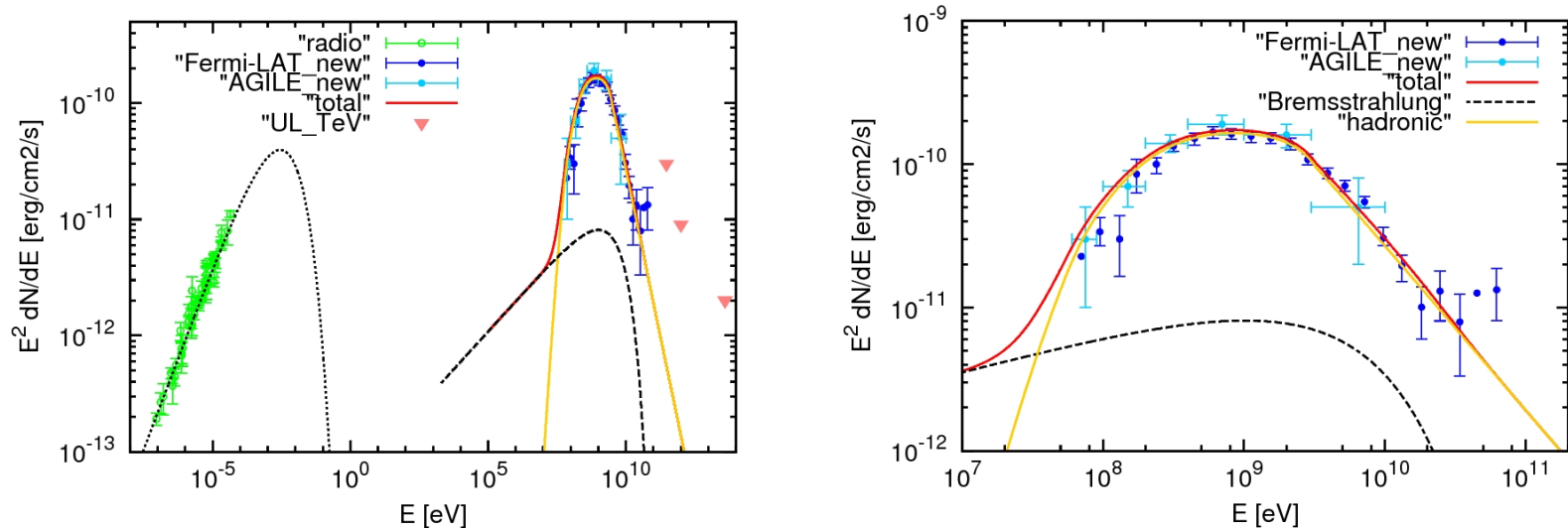


Fig. 4. Our best hadronic model, H3, of the broadband spectrum of the SNR W44 superimposed with radio (data points in green color) and gamma-ray data of Fig. 1 (in blue and cyan color). Proton distribution in Eq. (3) with index $p_1 = 2.2 \pm 0.1$ (for $E < E_{br}$) and $p_2 = 3.2 \pm 0.1$ (for $E > E_{br}$) where $E_{br}^p = 20$ GeV. This model is characterized by $B = 210 \mu\text{G}$ and $n = 300 \text{ cm}^{-3}$. The yellow curve shows the neutral pion emission from the accelerated proton distribution discussed in the text. The black curves show the electron contribution by synchrotron (dot) and bremsstrahlung (dashed) emissions; the IC contribution is negligible. The red curve shows the total gamma-ray emission from pion-decay and bremsstrahlung. *Left panel:* SED from radio to gamma-ray band. *Right panel:* only gamma-ray part of the spectrum.

Acceleration of cosmic rays at SNR

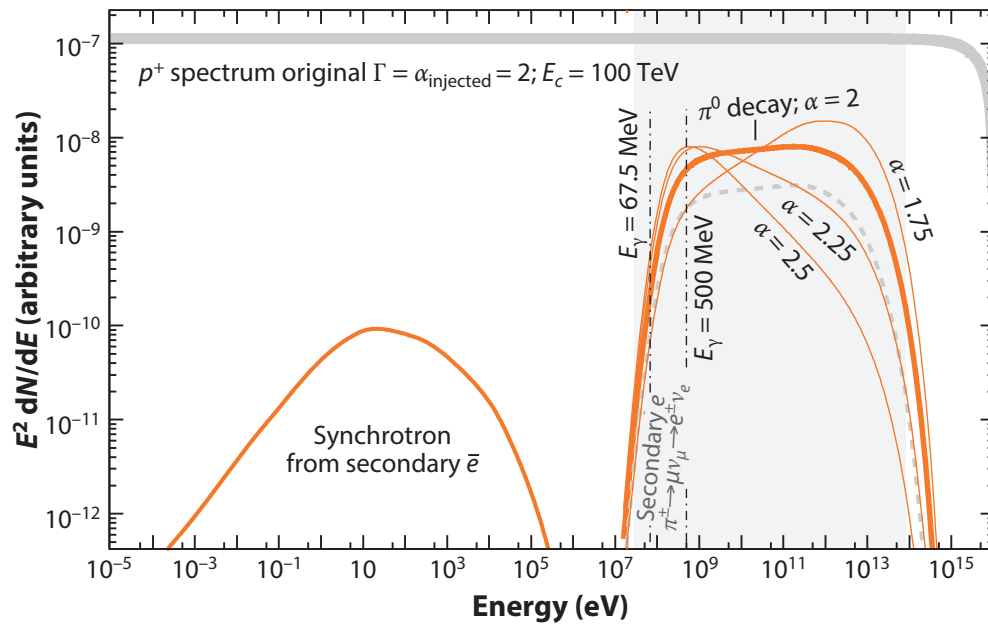


Figure 3

Spectral energy distribution of accelerated protons (power-law index $\alpha_{\text{injected}} = 2.0$ and cutoff at 100 TeV) and γ -rays resulting from inelastic collisions with interstellar material. The dominant emission into photons occurs via the decay $\pi^0 \rightarrow \gamma\gamma$ (solid orange curves). The γ -ray spectrum follows the parent protons' spectrum rather closely in the midenergy range and in the high-energy cutoff region. For all proton indices, the low-energy turnover is a characteristic feature of the pion-decay emission. Also shown is the spectrum of electrons resulting from the inelastic proton-proton interactions via the decay chain $\pi^\pm \rightarrow \mu + \nu_\mu \rightarrow e^\pm \nu_e$ (dashed gray curve). For the synchrotron emission from these so-called secondary electrons, a source with age $t_{\text{age}} = 1,000$ years and $B = 30 \mu\text{G}$ have been assumed. The shaded gray region shows the sensitive range of current γ -ray detectors (*Fermi*-LAT, imaging atmospheric Cherenkov detectors).

flux at Earth by an astrophysical accelerator that puts a fraction ϵ_{CR} of the energy output into the acceleration of protons:

$$F_\gamma(>100 \text{ MeV}) = 4.4 \times 10^{-7} \frac{\epsilon_{\text{CR}}}{\text{kpc}^2 \text{ s}^{-1}} \frac{E_{\text{pr}}}{10^{51} \text{ erg}}$$

In other words, if the distance d and the density of the interaction region n are known, the proton flux F_{pr} can be directly inferred from the γ -ray flux F_γ .

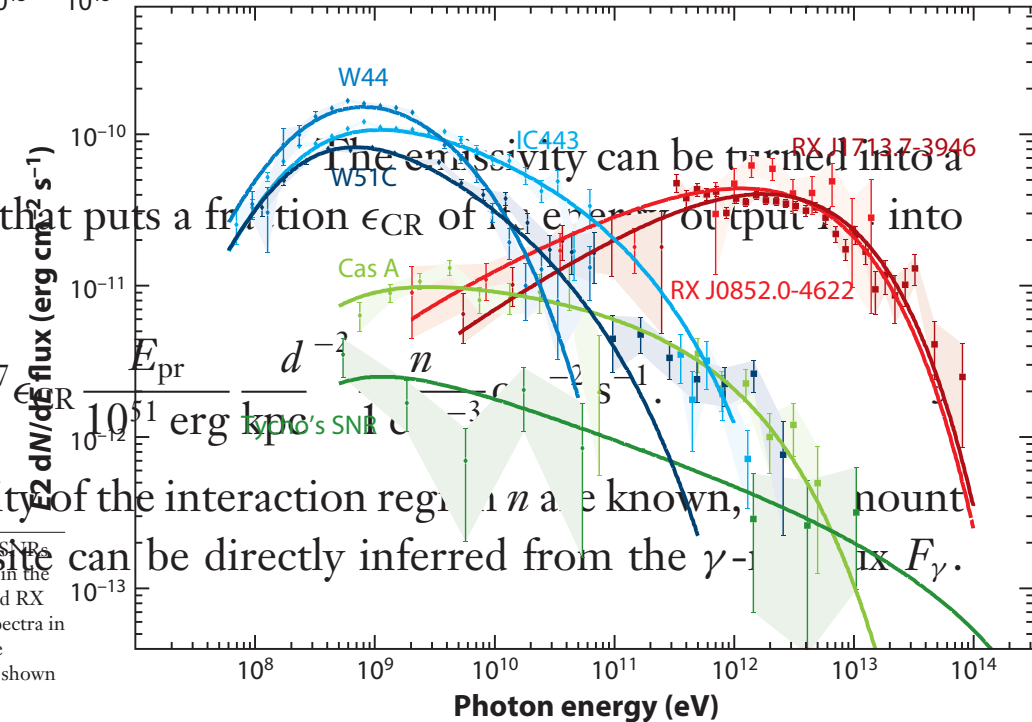


Figure 6

Typical γ -ray energy spectra for several of the most prominent supernova remnants (SNRs). Young SNRs ($< 1,000$ years) are shown in green. These typically show smaller γ -ray fluxes but rather hard spectra in the GeV and TeV bands. The older (but still referred to as young) shell-type SNRs RX J1713.7-3946 and RX J0852.0-4622 (Vela Junior) of ages $\sim 2,000$ years are shown in shades of red. These show very hard spectra in the GeV band ($\Gamma = 1.5$) and a peak in the TeV band with an exponential cutoff beyond 10 TeV. The middle-aged SNRs ($\sim 20,000$ years) interacting with molecular clouds (W44, W51C, and IC443) are shown in blue. Also shown are hadronic fits to the data (solid lines).

HESS: Acceleration of Petaelectronvolt protons in the Galactic Centre

Nature 531, 476 (2016)

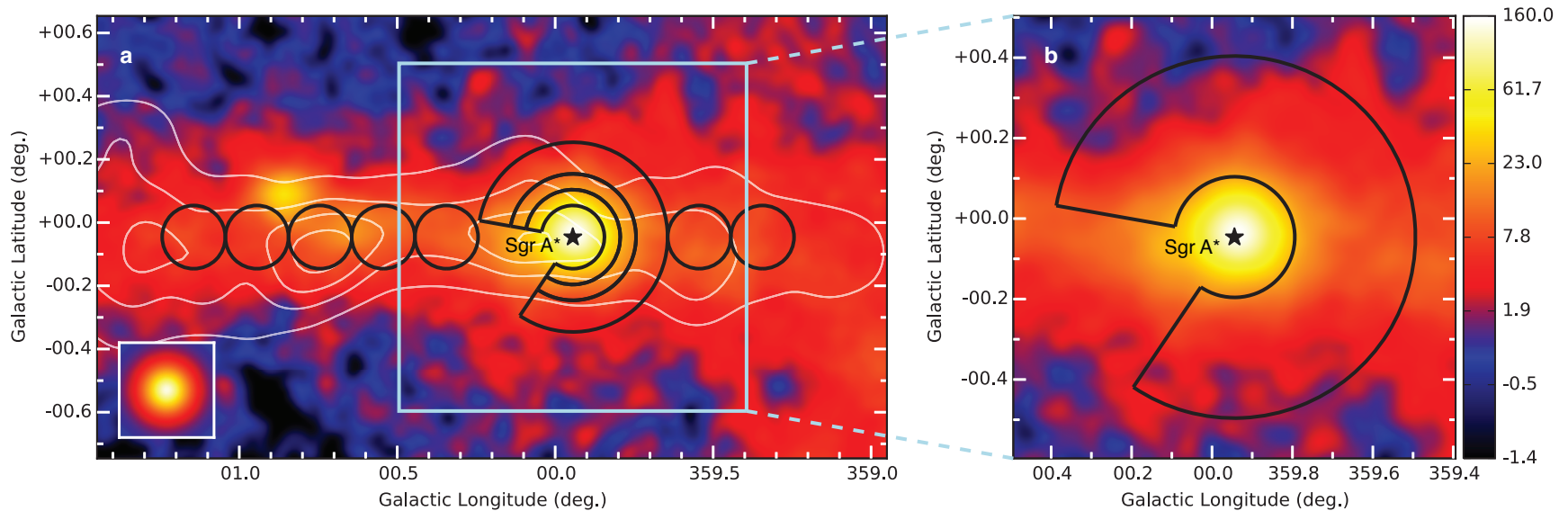


Figure 1: **VHE γ -ray image of the Galactic Centre region.** The colour scale indicates counts per $0.02^\circ \times 0.02^\circ$ pixel. *Left panel:* The black lines outline the regions used to calculate the CR energy density throughout the central molecular zone. A section of 66° is excluded from the annuli (see Methods). White contour lines indicate the density distribution of molecular gas, as traced by its CS line emission³⁰. The inset shows the simulation of a point-like source. *Right panel:* Zoomed view of the inner ~ 70 pc and the contour of the region used to extract the spectrum of the diffuse emission.

HESS: Acceleration of Petaelectronvolt protons in the Galactic Centre

Nature 531, 476 (2016)

Here we report deep gamma-ray observations with arcminute angular resolution of the Galactic Centre regions, which show the expected tracer of the presence of PeV particles within the central 10 parsec of the Galaxy. We argue that the supermassive black hole Sagittarius A* is linked to this PeVatron. Sagittarius A* went through active phases in the past, as demonstrated by X-ray outbursts and an outflow from the Galactic Center. Although its current rate of particle acceleration is not sufficient to provide a substantial contribution to Galactic cosmic rays, **Sagittarius A*** could have plausibly been more active over the last $\sim 10^6\text{--}7$ years, and therefore **should be considered as a viable alternative to supernova remnants as a source of PeV Galactic cosmic rays.**

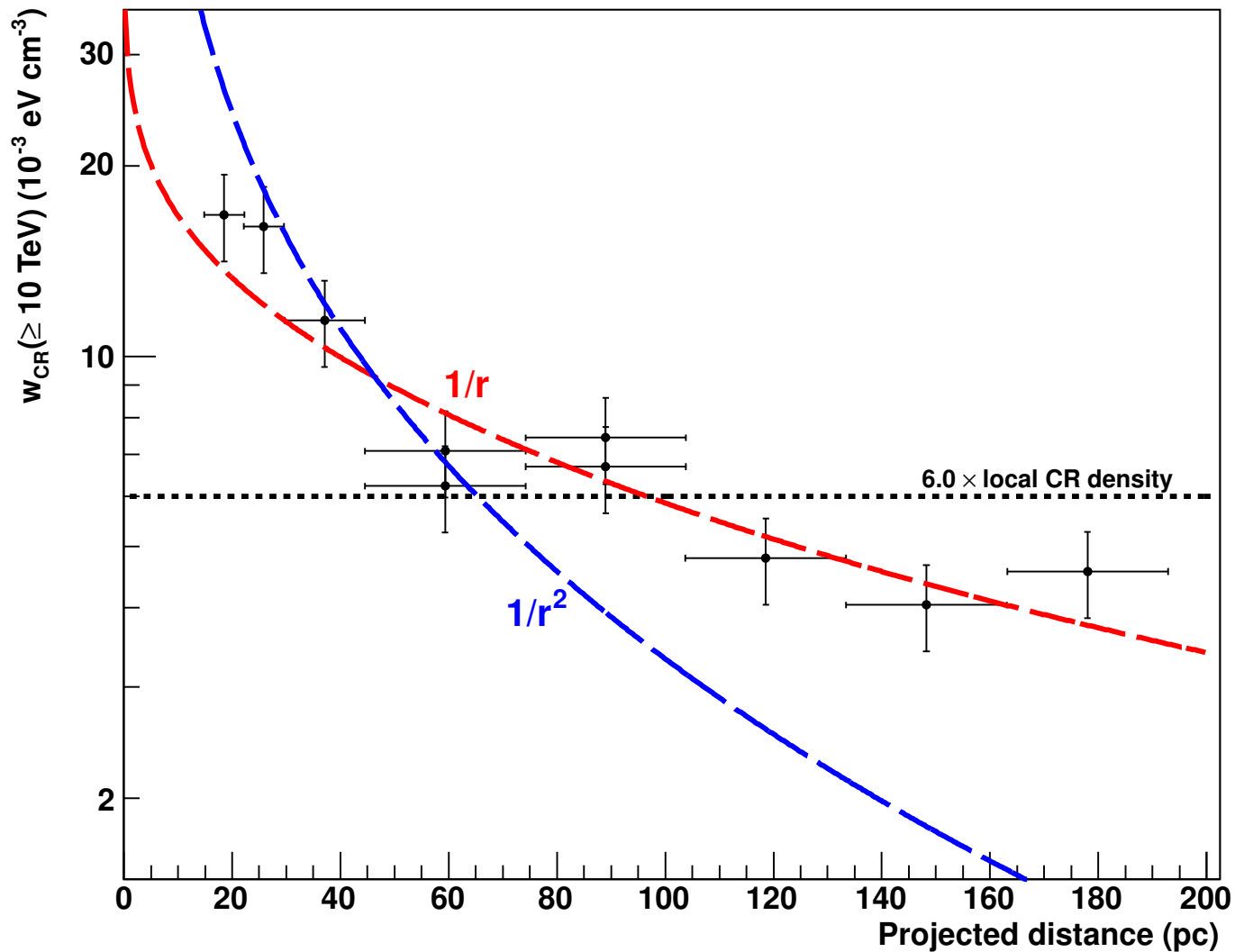


Figure 2: **Spatial distribution of the CR density versus projected distance from Sgr A***. The vertical and horizontal error bars show the 1σ statistical plus systematical errors and the bin size, respectively. A fit to the data of a $1/r$ (red line, $\chi^2/\text{d.o.f.} = 11.8/9$), $1/r^2$ (blue line, $\chi^2/\text{d.o.f.} = 73.2/9$) and an homogeneous (black line, $\chi^2/\text{d.o.f.} = 61.2/9$) CR density radial profiles integrated along the line of sight are shown. The best fit of a $1/r^\alpha$ profile to the data is found for $\alpha = 1.10 \pm 0.12$ (1σ). The $1/r$ radial profile is clearly preferred by the H.E.S.S. data.

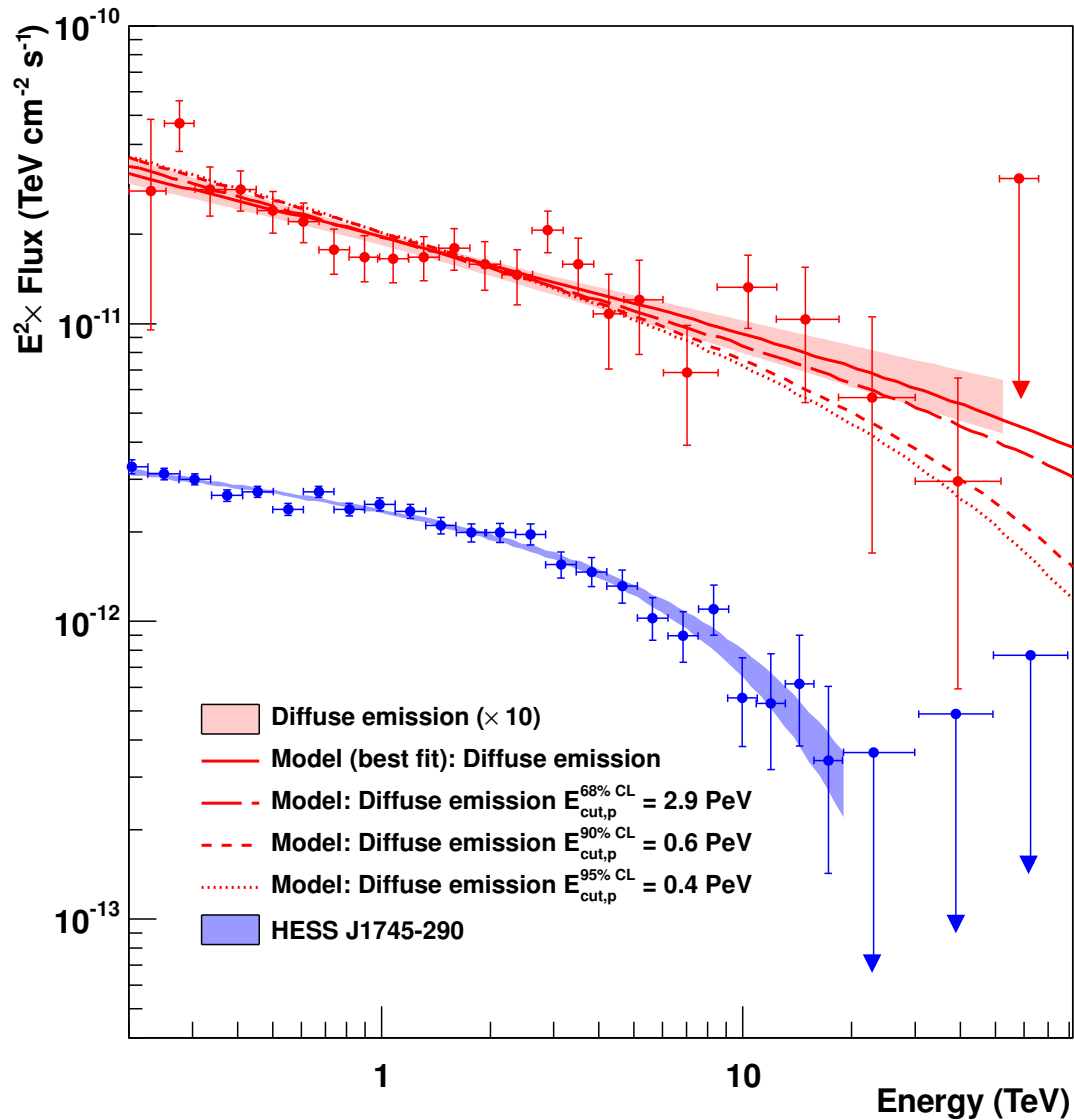
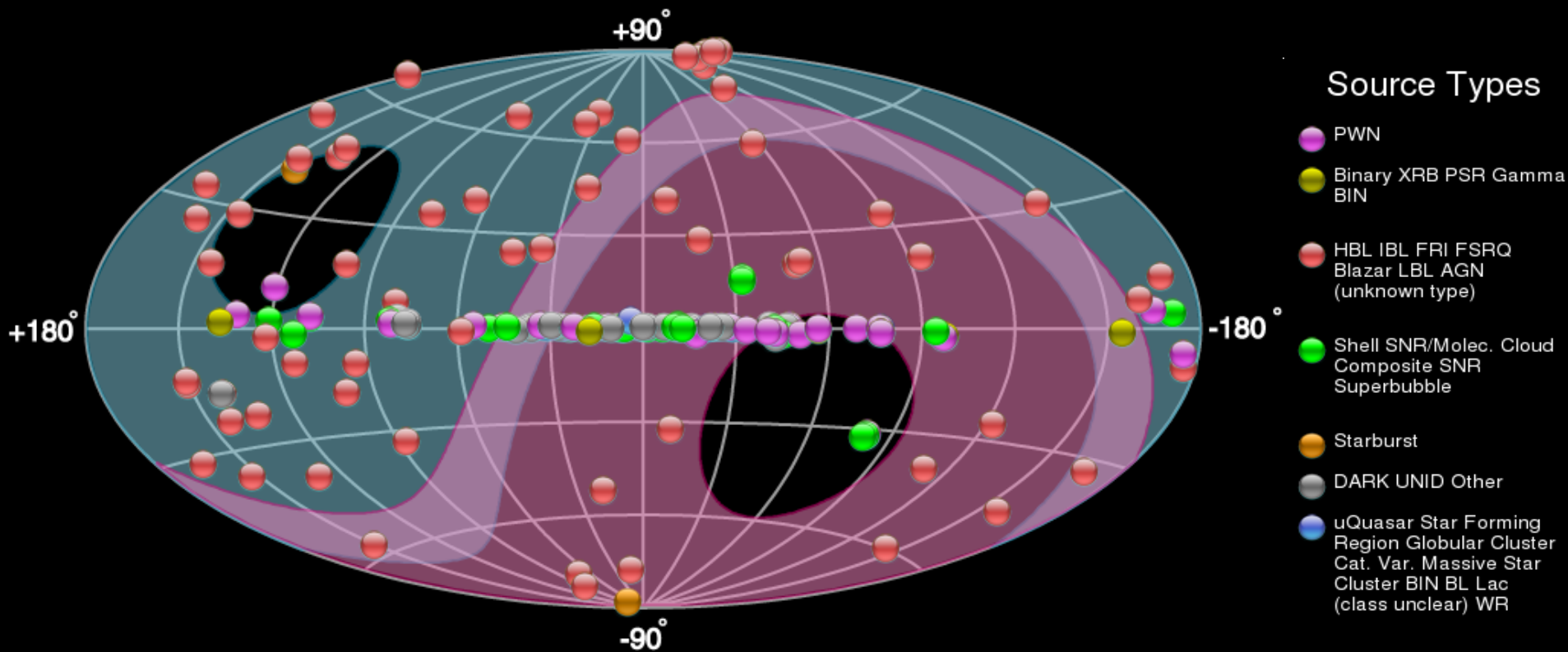


Figure 3: **VHE γ -ray spectra of the diffuse emission and HESS J1745-290.** The Y axis shows fluxes multiplied by a factor E^2 , where E is the energy on the X axis, in units of $\text{TeV cm}^{-2} \text{s}^{-1}$. The vertical and horizontal error bars show the 1σ statistical error and bin size, respectively. Arrows represent 2σ flux upper limits. The 1σ confidence bands of the best-fit spectra of the diffuse and HESS J1745-290 are shown in red and blue shaded areas, respectively. Spectral parameters are given in Methods. The red lines show the numerical computations assuming that γ -rays result from the decay of neutral pions produced by proton-proton interactions. The fluxes of the diffuse emission spectrum and models are multiplied by 10.

The TeV sky today: a large variety of sources

Already 162 detected sources reported in the TeV Catalog in August 2015 !
65 sources are extragalactic - 70 are Galactic - 27 UNID



2) extragalactic sources

1997 discovery of strong variations of the flux of Mrk 421 + Mrk 501

Burst with $\sim 30\%$ intensity change within a day.

Some changes on 15 min time scales.

Time scale of variability constrains the size of the

source: $\Delta x \approx c \cdot \Delta \tau \sim$ size of solar system

$$\approx 1h$$

Objects are far away $D = \frac{z \cdot c}{H_0} \approx \frac{0.033 \cdot 3 \cdot 10^5 \frac{\text{km}}{\text{s}}}{65 \frac{\text{km}}{\text{s Mpc}}} \approx 150 \text{ Mpc}$

estimate proton density at source:

$$n_\gamma \approx 10^{12} - 10^{15} \frac{1}{\text{cm}^3} \text{ in the TeV range}$$

problem: at such energies the photon field is not

transparent any more above 10 TeV

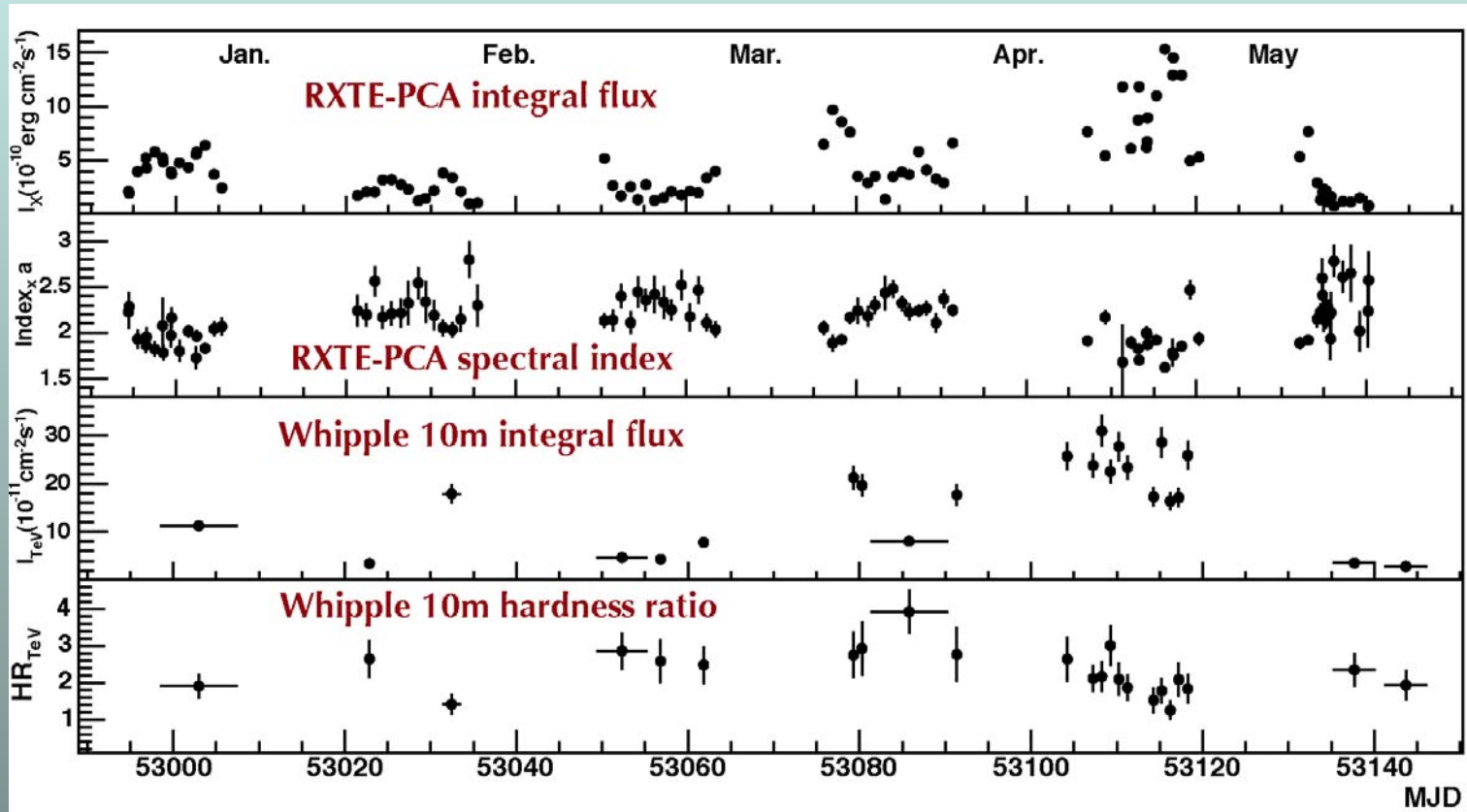
threshold:

$$\gamma\gamma \rightarrow e^+e^-$$

$$4E_\gamma \epsilon_\gamma > (2m_e c^2)^2 = 10^{12} \text{ eV}^2$$

OG 2.3: Extragalactic Sources

Mkn 421



Whipple [Grube]:

2004: Five month multi- λ campaign: X-ray, TeV γ -ray.

Multiwavelength campaign of Mkn 421

Another famous, close-by and bright blazar

January 2013 flare:

162, 787, 1118

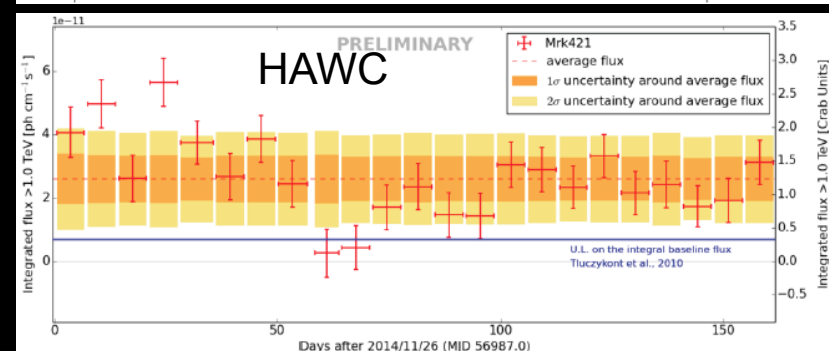
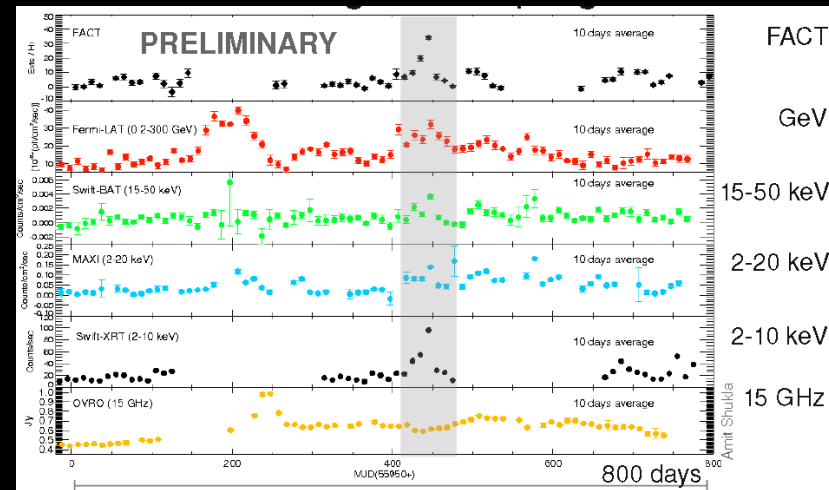
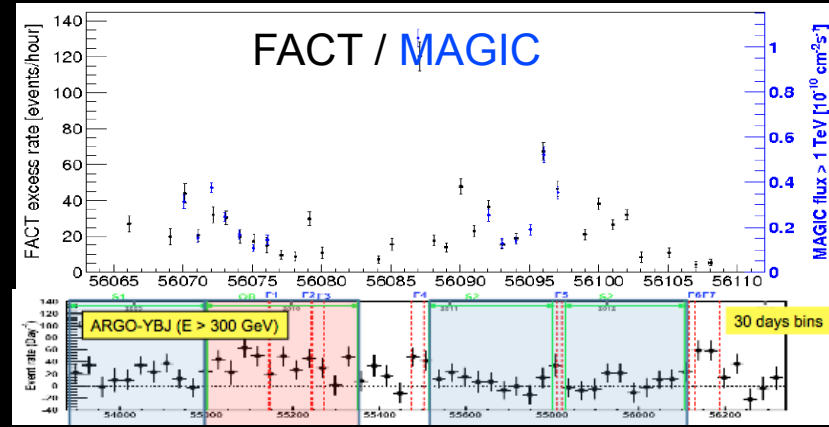
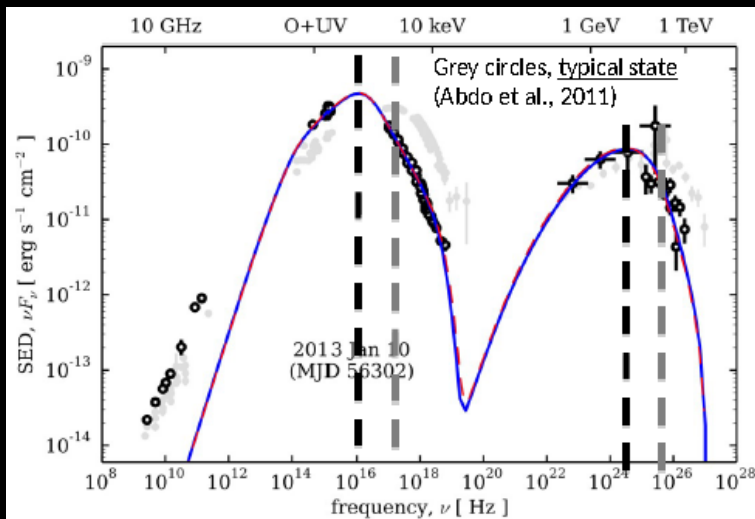
Synchrotron and IC peak shifted to ~ 10 times lower energies

\Rightarrow Never seen before for any blazar

4.5 year campaign also followed by ARGO-YBJ

Variability clearly detected by HAWC

Deep monitoring by FACT



solution: relativistic beaming

Source moves towards us at relativistic speeds.

In moving coordinate system

$$R' = \gamma \cdot R$$

i.e.

$$E' = \frac{1}{\gamma} \cdot E$$

1) the volume is a factor γ larger

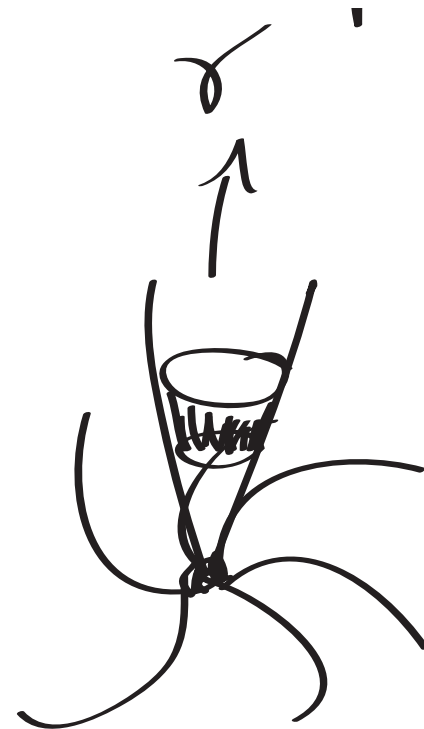
2) the energy is a factor $1/\gamma$ smaller

--> the threshold is increased by a factor γ^2

since we observe photons at $E > 10 \text{ TeV}$

$$\Rightarrow \gamma > 30$$

i.e. relativistic jet is moving towards us



Radio Imaging of the Very-High-Energy γ -Ray Emission Region in the Central Engine of a Radio Galaxy

The VERITAS Collaboration, the VLBA 43 GHz M87 Monitoring Team, the H.E.S.S. Collaboration, the MAGIC Collaboration*

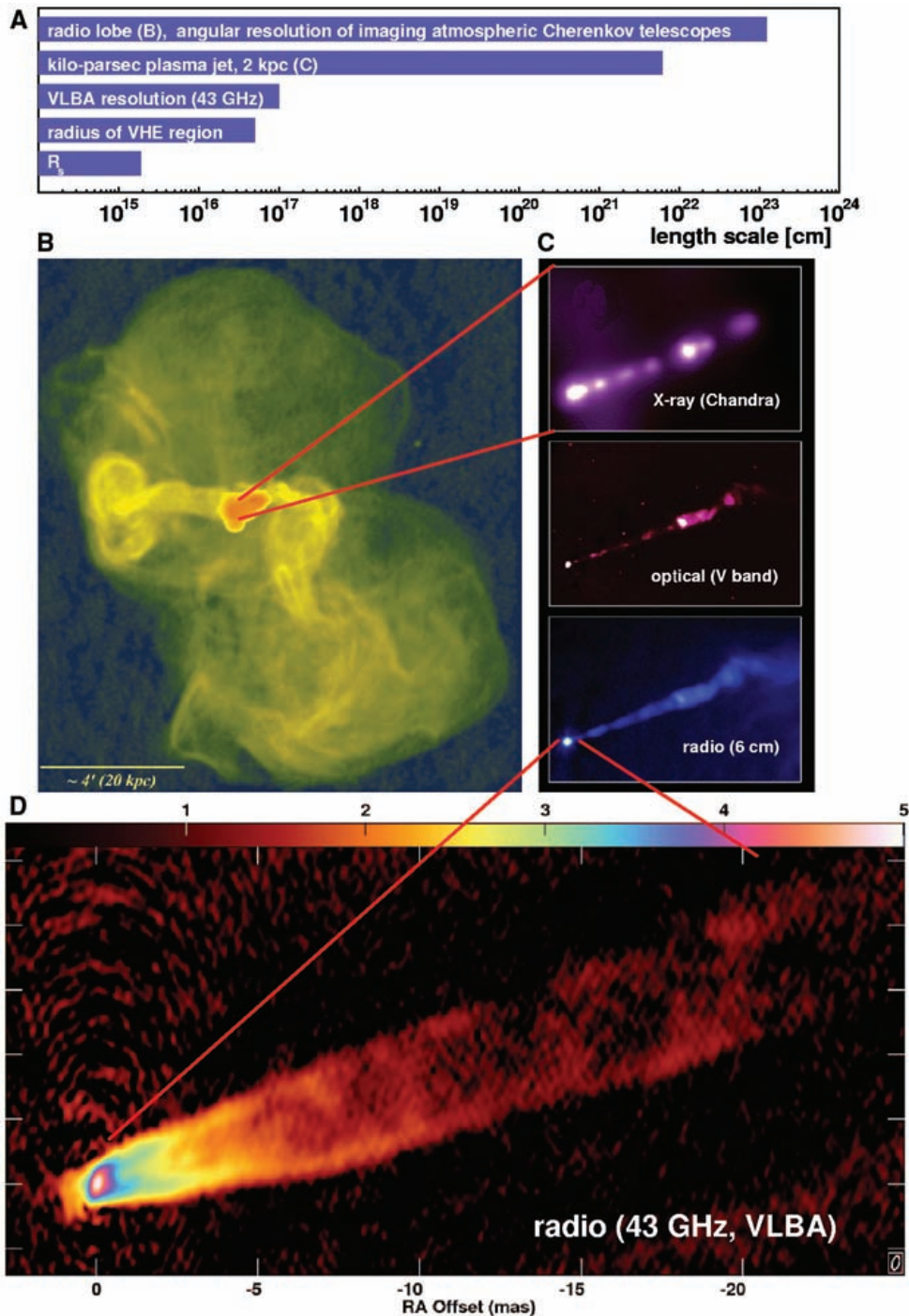
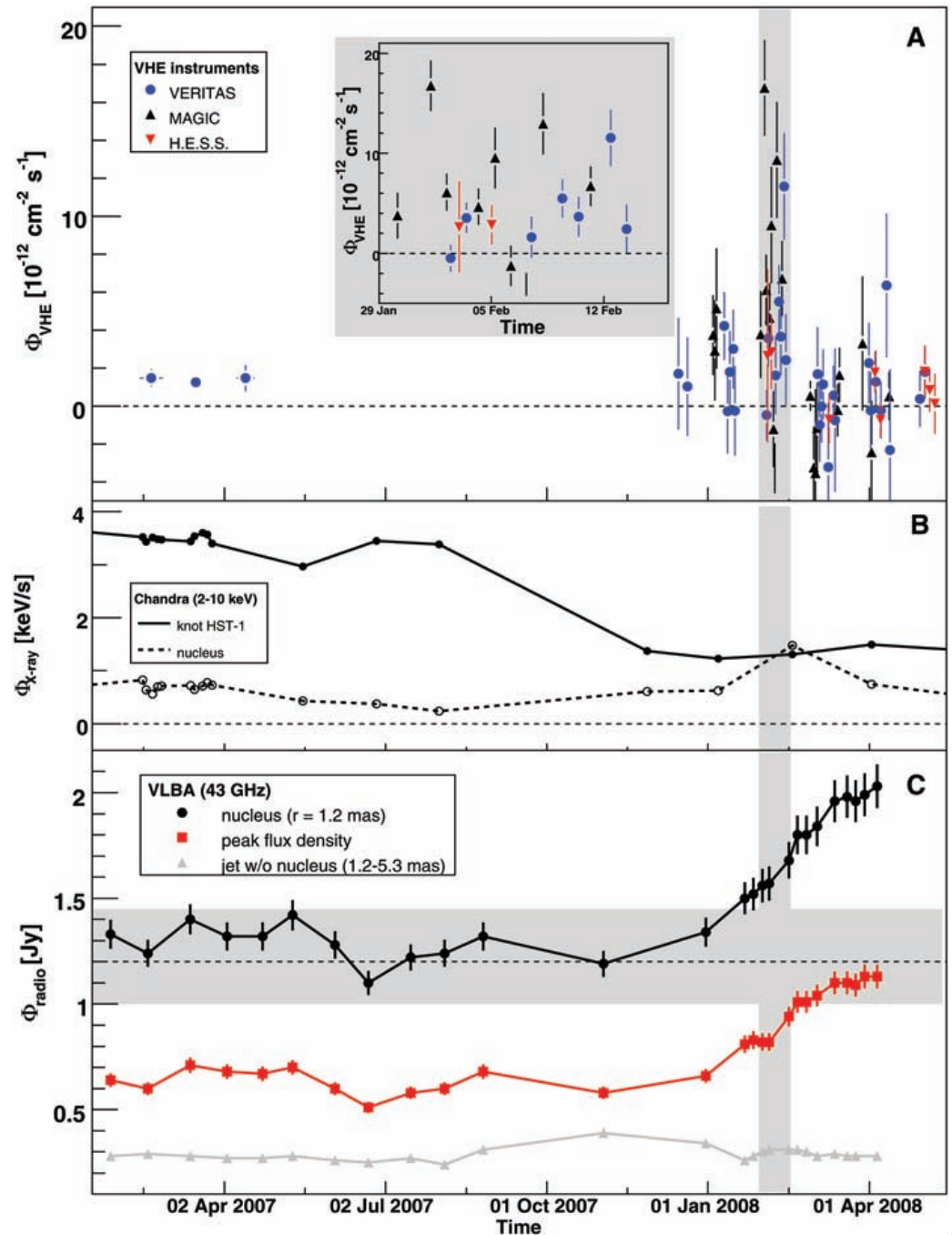


Fig. 1. M87 at different photon frequencies and length scales. **(A)** Comparison of the different length scales. **(B)** 90-cm radio emission measured with the VLA. The jet outflows terminate in a halo that has a diameter of ~ 80 kpc ($15'$). The radio emission in the central region is saturated in this image. [Credit: F. N. Owen, J. A. Eilek, and N. E. Kassim (32), NRAO/Associated Universities Incorporated/NSF] **(C)** Zoomed image of the plasma jet with an extension of 2 kpc ($20''$), seen in different frequency bands: x-rays (Chandra, top), optical (V band, middle), and radio (6 cm, bottom). Individual knots in the jet and the nucleus can be seen in all three frequency bands. The innermost knot HST-1 is located at a projected distance of 0.86 arc sec (60 pc, $\approx 10^5 R_s$) from the nucleus. [Credit: x-ray, NASA/Chandra X-Ray Observatory Science Center/Massachusetts Institute of Technology/H. Marshall *et al.*; radio, F. Zhou, F. Owen (NRAO), J. Biretta (Space Telescope Science Institute); optical, NASA/STScI/University of Maryland Baltimore County/E. Perlman *et al.* (8)] **(D)** An averaged, and hence smoothed, radio image based on 23 images from the VLBA monitoring project at 43 GHz. The color scale gives the logarithm of the flux density in units of 0.01 millijansky per beam. The indication of a counter-jet can be seen, emerging from the core toward the lower left side. mas, milli-arc seconds.

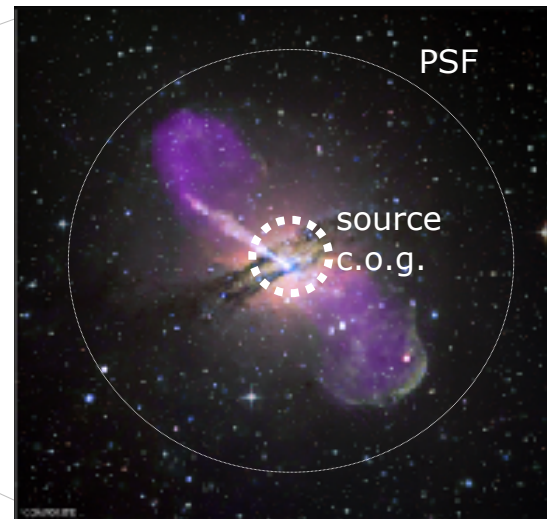
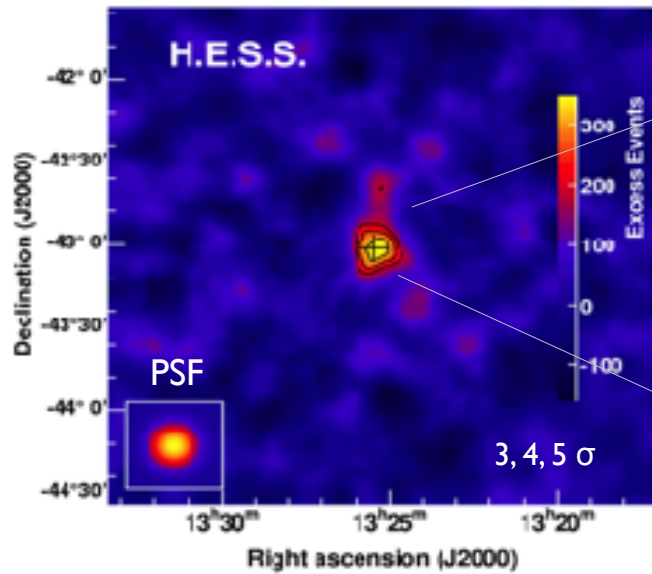
Radio Imaging of the Very-High-Energy γ -Ray Emission Region in the Central Engine of a Radio Galaxy

The VERITAS Collaboration, the VLBA 43 GHz M87 Monitoring Team, the H.E.S.S. Collaboration, the MAGIC Collaboration*



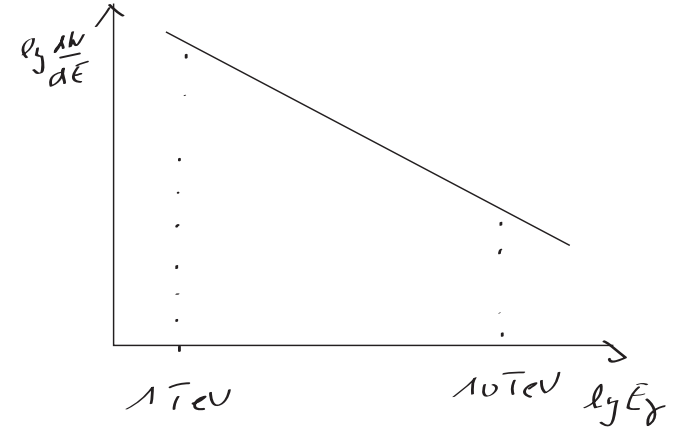
Centaurus A

d~3.8 Mpc



Energy spectrum of Mrk 421 & Mrk 501

At high energies we expect absorption of gamma rays at photons of 3K microwave background



$$\gamma_{\text{TeV}} + \gamma_{3\text{K}} \rightarrow e^+ e^-$$

threshold:

$$\epsilon_{\gamma} \cdot E_{\gamma} (1 - \cos \Theta) > 2(m_e \cdot c^2)^2$$

3 K
IR

0.16 meV
0.5 eV

3 PeV
1 TeV

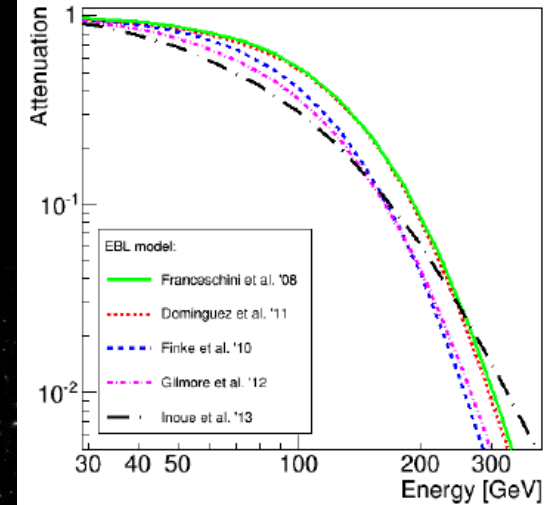
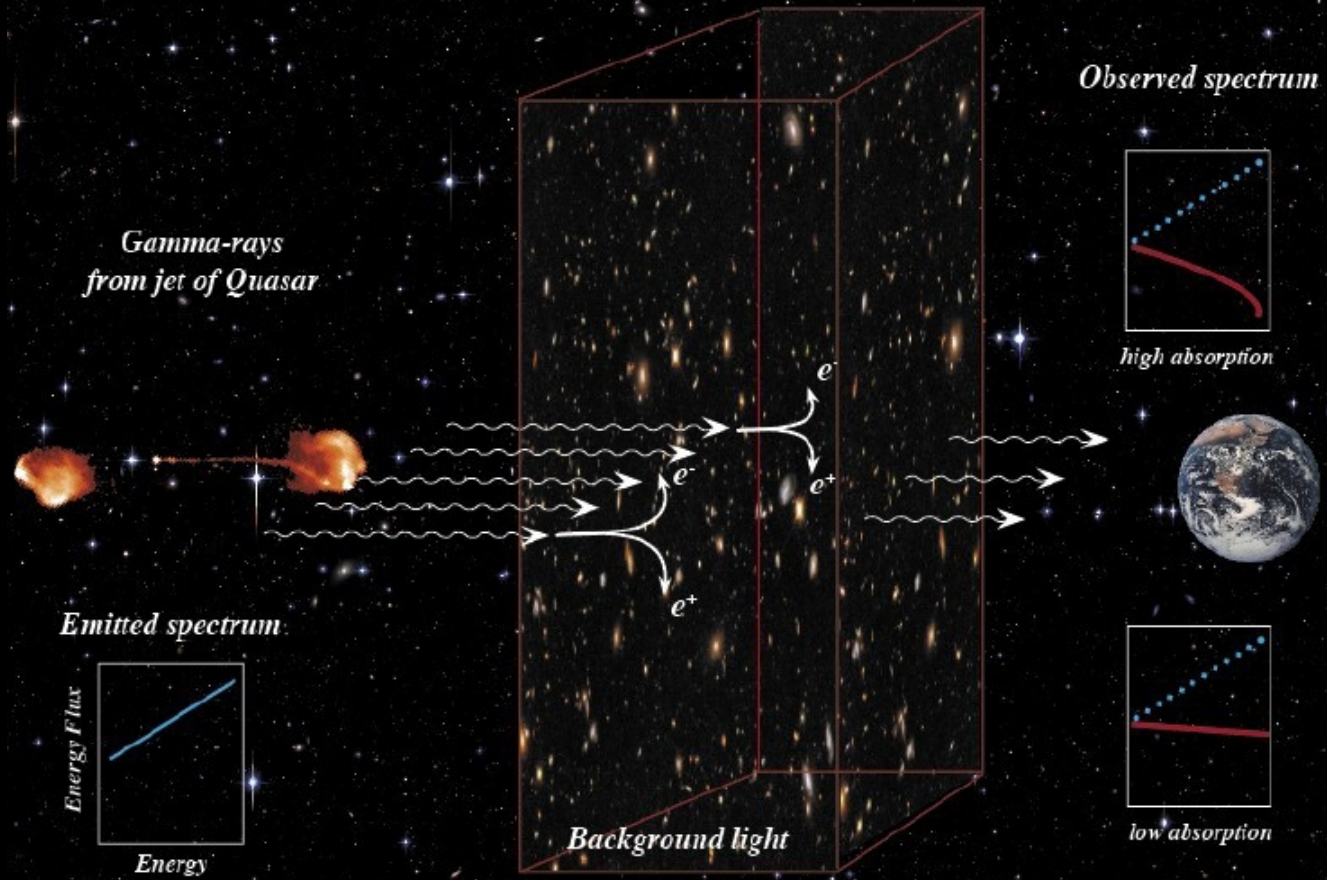
← **measure the density of the IR background**

important for cosmology:
high: early galaxy formation
low: late galaxy formation

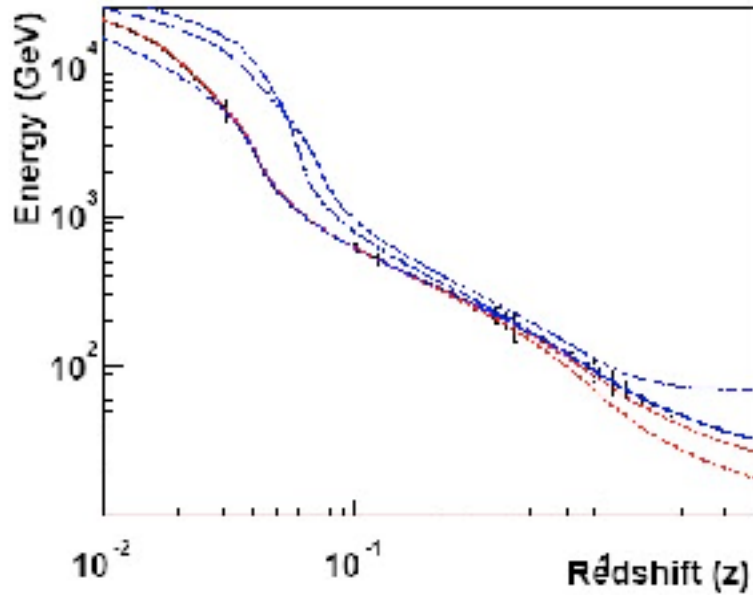
Absorption by the Extragalactic Background Light

Sources with $z \sim 1$ strong absorption above 100 GeV

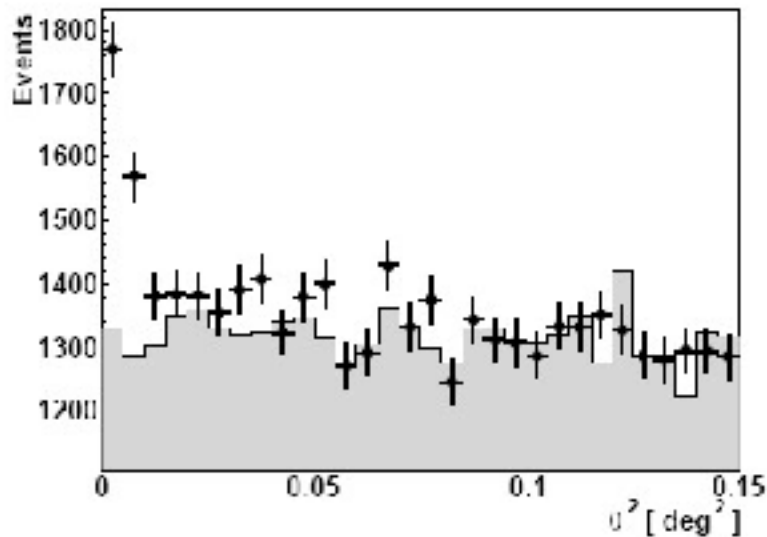
GeV+TeV spectrum can be used for testing EBL models



The Blazar 1ES 1101-232 and the Gamma Ray Horizon



The "gamma ray horizon" defined as the distance (measured in redshift z) over which a gamma ray of a given energy will typically propagate before interacting with a photon of the extragalactic background light (from [Blanch and Martinez, 2005](#)). Different lines correspond to different models (and time scales) of galaxy formation, resulting in varying levels of background light.



Angular distribution of gamma-ray candidates detected by H.E.S.S. relative to the direction towards 1ES 1101-232. The gray area gives an estimate of the uniform background from cosmic-ray showers. The excess from the source has a significance of more than 11 standard deviations.

H.E.S.S.

The Blazar 1ES 1101-232 and the Gamma Ray Horizon

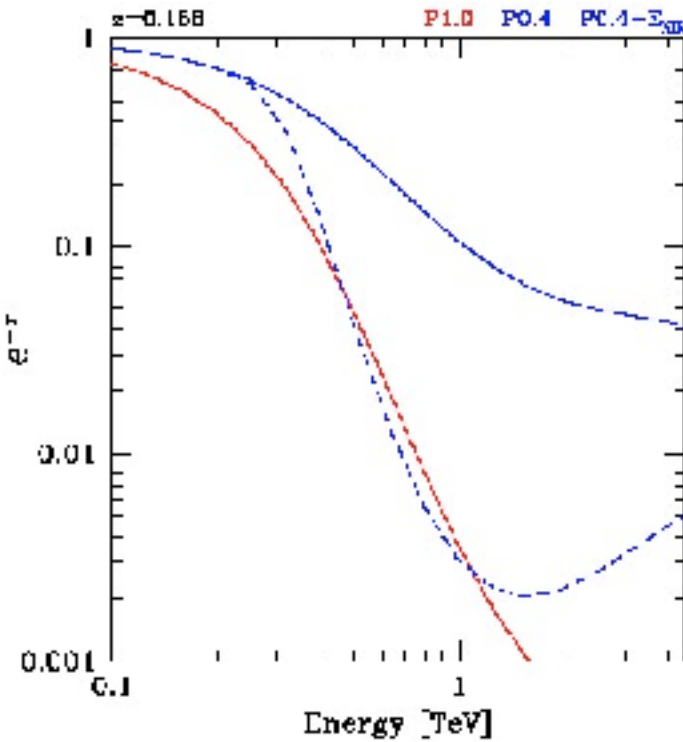
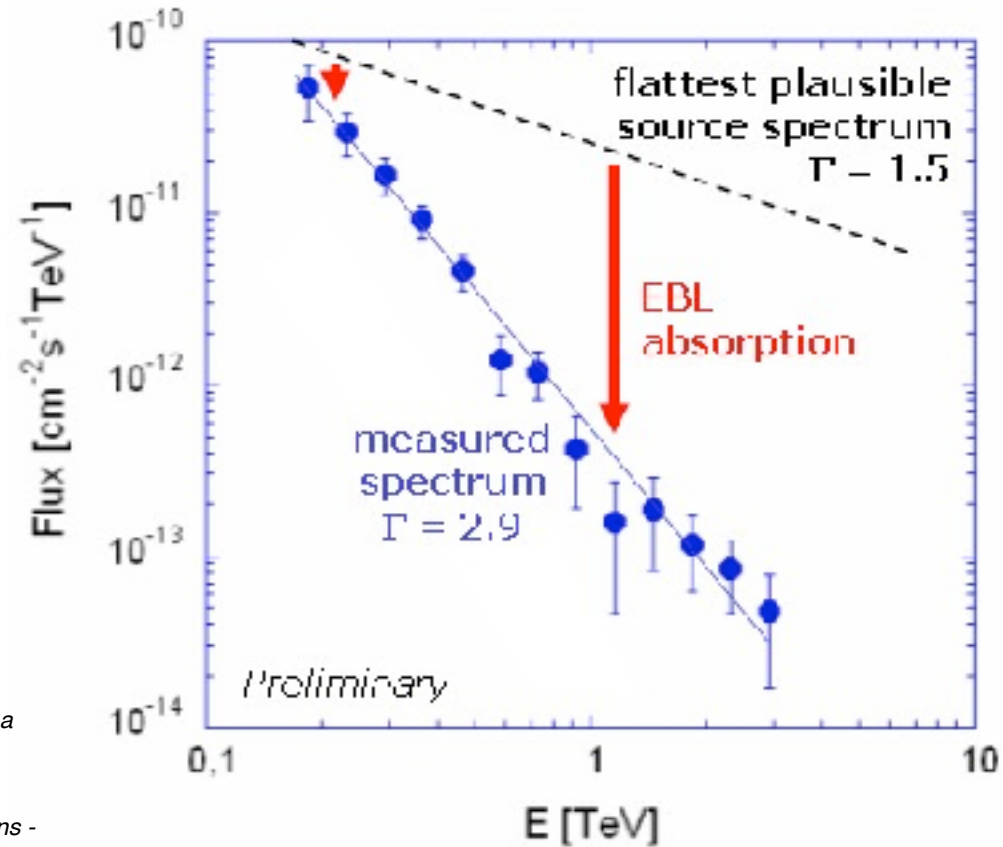


Fig. 2: Absorption of gamma rays from 1ES 1101-232 as a function of gamma-ray energy. The red curve shows the effect of typically assumed EBL levels, the blue curve the minimal EBL corresponding to the light of detected galaxies. The dashed curve indicates the effect of an additional near-infrared bump, as suggested by some direct EBL measurements.

H.E.S.S.

Fig. 3: Energy spectrum of gamma rays from 1ES 1101-232. The spectrum has a spectral index of 2.9. The dashed line indicates the flattest plausible spectrum generated by the AGN. Given that at low energies - around 0.1-0.2 TeV - the absorption of gamma rays has to be small - lacking appropriate UV target photons - absorption at 1 TeV has to be well below a factor 100, ruling out EBL models like the ones indicated by the red line or the dashed blue line in Fig. 2.



Breaking the redshift barrier with PKS 1441+25 => Constraints on the EBL

868, 1220, 1336

FSRQ @ $z = 0.939$

MAGIC detection

VERITAS Confirmation

Up to 200 GeV

~400 GeV accounting for $z!$

Stringent constraints on the EBL

